Kinetics of Ligand Binding to Receptor Immobilized in a Polymer Matrix, as Detected with an Evanescent Wave Biosensor. I. A Computer Simulation of the Influence of Mass Transport

Peter Schuck
Section of Physical Biochemistry, Laboratory of Biochemical Pharmacology, National Institute of Diabetes, Digestive and Kidney Diseases, National Institutes of Health, Bethesda, Maryland 20892 USA

ABSTRACT The influence of mass transport on ligand binding to receptor immobilized in a polymer matrix, as detected with an evanescent wave biosensor, was investigated. A one-dimensional computer model for the mass transport of ligand between the bulk solution and the polymer gel and within the gel was employed, and the influence of the diffusion coefficient, the partition coefficient, the thickness of the matrix, and the distribution of immobilized receptor were studied for a variety of conditions. Under conditions that may apply to many published experimental studies, diffusion within the matrix was found to decrease the overall ligand transport significantly. For relatively slow reactions, small spatial gradients of free and bound ligand in the gel are found, whereas for relatively rapid reactions strong inhomogeneities of ligand within the gel occur before establishment of equilibrium. Several types of deviations from ideal pseudo-first-order binding progress curves are described that resemble those of published experimental data. Extremely transport limited reactions can in some cases be fitted with apparently ideal binding progress curves, although with apparent reaction rates that are much lower than the true reaction rates. Nevertheless, the ratio of the apparent rate constants can be semiquantitatively consistent with the true equilibrium constant. Apparently "cooperative" binding can result from high chemical on rates at high receptor saturation. Dissociation in the presence of transport limitation was found to be well described empirically by a single or a double exponential, with both apparent rate constants considerably lower than the intrinsic chemical rate constant. Transport limitations in the gel can introduce many generally unknown factors into the binding progress curve. The simulations suggest that unexpected deviations from ideal binding progress curves may be due to highly transport influenced binding kinetics. The use of a thinner polymer matrix could significantly increase the range of detectable rate constants.

INTRODUCTION

During the last several years, evanescent wave biosensors have become increasingly popular for determining the affinity and kinetics of interactions of biological macromolecules. The optical biosensors that measure refractive index changes caused by bound macromolecules permit one to monitor the time dependence of the binding of label-free macromolecules to receptors immobilized on a surface. They are used to study binding in a number of different fields, e.g., antigen-antibody interactions, protein-protein interactions, protein-DNA interactions, and virus research (see, e.g., the reviews of Fisher and Fivash, 1994, and Malmborg and Borrebaeck, 1995, and the references cited therein).

The operation of these biosensors is based on the optical properties of thin films with high refractive index deposited on a glass surface. Light coming from the glass is totally internally reflected, and at a certain angle of incidence the excitation of resonance in the film produces intensity and phase changes in the reflected beam. For the measurement one exploits the fact that the resonance characteristic is very sensitive to changes of the refractive index in the evanescent field, which extends, exponentially decaying, into the volume above the sensor surface. For a more detailed description of the physics see Cush et al. (1993) and Raether (1977). Two types are currently commercially available, a surface plasmon resonance biosensor (BIACORE and BIALITE; Pharmacia Biosensor AB, Uppsala, Sweden) (Löfås et al., 1991) and a waveguide (or resonant mirror) biosensor (IASYS; Fisons Applied Sensor Technology, Cambridge, England) (Buckle et al., 1993; Cush et al., 1993).

In most of the published experiments the receptor is covalently coupled to a flexible hydrogel matrix, which is attached via a linker layer to the sensor surface (Löfås and Johnsson, 1990). This hydrogel matrix is composed of carboxymethylated dextran chains and has a thickness of 100–200 nm (Johnsson et al., 1995). The advantages of using the dextran matrix are prevention of proteins from coming into contact with the metal surface, minimizing nonspecific adsorption, providing better accessibility of immobilized receptors to the substrate, and increased sensitivity due to higher amounts of immobilized receptors (Liedberg et al., 1993; Löfås and Johnsson, 1990). However, the possible disadvantages of such a matrix have not been considered heretofore.

One observation common to many (O'Shannessy, 1994) or even most (Karlsson et al., 1994; Fisher et al., 1994) of the applications is that the observed binding and dissociation kinetics apparently do not follow a simple ideal pseudo-

Received for publication 5 September 1995 and in final form 20 November 1995.

Address reprint requests to Dr. Peter Schuck, National Institutes of Health, NIDDK, Bldg. 8, Rm. 220, 9000 Rockville Pike, Bethesda, MD 20892. Tel.: 301-594-1954; Fax: 301-402-0240; E-mail: pschuck@helix.nih.gov.

0006-3495/96/03/1230/20 $2.00

first-order binding progress curve (as described in the Appendix). Among other deviations, most of the published data show multiphasic association or dissociation phases. In addition, apparent cooperative binding (Fisher et al., 1994) and dependence on the choice of which binding partner is immobilized (Morton et al., 1994; Malmborg et al., 1992) have been described and remained mostly unexplained. Compared with other methods, lower rate constants (Ito and Kurosawa, 1993; Chaiken et al., 1992) and different equilibrium constants (up to 4 orders of magnitude; Guichard et al., 1994) have been reported. In the present study the diffusion/reaction process within the gel matrix is investigated as a source of some of these reported phenomena.

It is well known that reaction rate constants of biomolecules can be very high. In antibody reactions, chemical on rates up to 10^8 $M^{-1}s^{-1}$ have been observed (Foote and Milstein, 1991; Felder et al., 1993). Accordingly, the influence of diffusion on the kinetics of protein surface binding in biological systems and biosensors is very important and has drawn much theoretical attention (e.g., Goldstein and Dembo, 1995; Balgi et al., 1995; Zwanzig and Szabo, 1991; Hsieh and Thompson, 1994). For the surface plasmon resonance biosensor, ligand transport in the laminar flow of the bulk phase toward the sensor surface and its effects on the measured kinetics have been investigated by Glaser (1993). Additionally, Karlsson et al. (1994) described the transition from reaction-limited to transport-limited binding, assuming steady-state conditions. However, common to all studies concerning the surface plasmon resonance biosensor is the assumption that ligands bind to an idealized planar array of sites, i.e., an array that is two-dimensional on the molecular scale. Consequently, the transport processes are dependent on the buffer flow rate, which in turn was thought to provide an experimental tool for the important problem of diagnosing transport limitation (Fägerstam et al., 1992; Glaser, 1993; Malmborg et al., 1992; Chaiken et al., 1992; Kelley, 1994).

In the present work a rather different and considerably more realistic model of the binding process is presented and explored. The array of binding sites within the polymer matrix is treated as three-dimensional rather than two-dimensional on the molecular scale. In particular, we explore the transport of ligand within the finite volume where the receptor is immobilized. Although this volume has a thickness of only 100–200 nm, the presence of immobilized receptor and high reaction rates can significantly hamper the transport process (Crank, 1975). The present model is also novel in incorporating exponentially decaying detection sensitivity of the evanescent wave (Kooyman et al., 1988; Stenberg et al., 1991; Liedberg et al., 1993). The sensitivity has a decay length comparable to the thickness of the gel matrix (Liedberg et al., 1993), and the measured signal is therefore sensitive to inhomogeneities of the bound ligand within the matrix.

To study the distribution of free and bound ligand in the gel matrix as a function of time and to calculate the corresponding biosensor signal, computer simulations were performed. The computational effort of the simulation was minimized by reducing the diffusion/reaction model to one dimension perpendicular to the sensor- surface (Fig. 1). This is believed to exhibit all characteristic effects of the finite thickness of the receptor layer, and it enabled the variation of many experimental parameters. In this way, the influence of the size of the gel, the receptor distribution, the partition coefficient of the ligand into the gel, the diffusion coefficient, and the decay length of the evanescent wave were investigated for a number of different equilibrium constants, chemical rate constants, bulk ligand concentrations, and levels of receptor immobilization. To account for the transport of the ligand into the gel, the ligand flux from the bulk into the gel matrix was approximated by assuming a constant transport coefficient, which was derived from steady-state conditions of the external mass transport in the laminar flow. It is assumed for simplicity that the optical properties of the sensor are constant, and that the properties of the gel are homogeneous and independent of the amount of bound macromolecules.

In the Discussion, we will attempt to demonstrate that the calculated effects of mass transport of ligand within the gel are significant in real experiments. Perhaps the most important aspect is the inverse problem: How can biosensor data be properly analyzed, and what qualitative conclusions can we draw from mass-transport-influenced kinetics? Using the results obtained here, these issues are addressed in a subsequent communication (Schuck, manuscript submitted for publication).

THE SIMULATION MODEL

In the model, it was assumed that the concentrations of receptor and free and bound ligand are constant in planes parallel to the sensor surface and vary only along the axis perpendicular to the sensor surface. With a given linear density of immobilized receptor $r(z)$, the time course of the distributions of free ligand $f(z, t)$ and bound ligand $b(z, t)$ can be described by a one-dimensional diffusion/reaction equation, where the reaction is assumed to be reversible and of pseudo-first-order:

$$\frac{\partial f}{\partial t} = D\frac{\partial^2 f}{\partial z^2} - \frac{\partial b}{\partial t} \tag{1a}$$

$$\frac{\partial b}{\partial t} = k_+\gamma f(r - b) - k_- b, \tag{1b}$$

where D denotes the diffusion coefficient, γ the activity coefficient of the ligand inside the gel, and k_+, k_- the chemical on rate and off rate constants, respectively) (Crank, 1975). The gel extends from the sensor surface at $z = 0$, which represents an impermeable wall, to the bulk solution at $z = G$, where material transport into and out of the gel takes place. Receptor can be present within the gel and on its surface; initially no ligand is present. Hence the

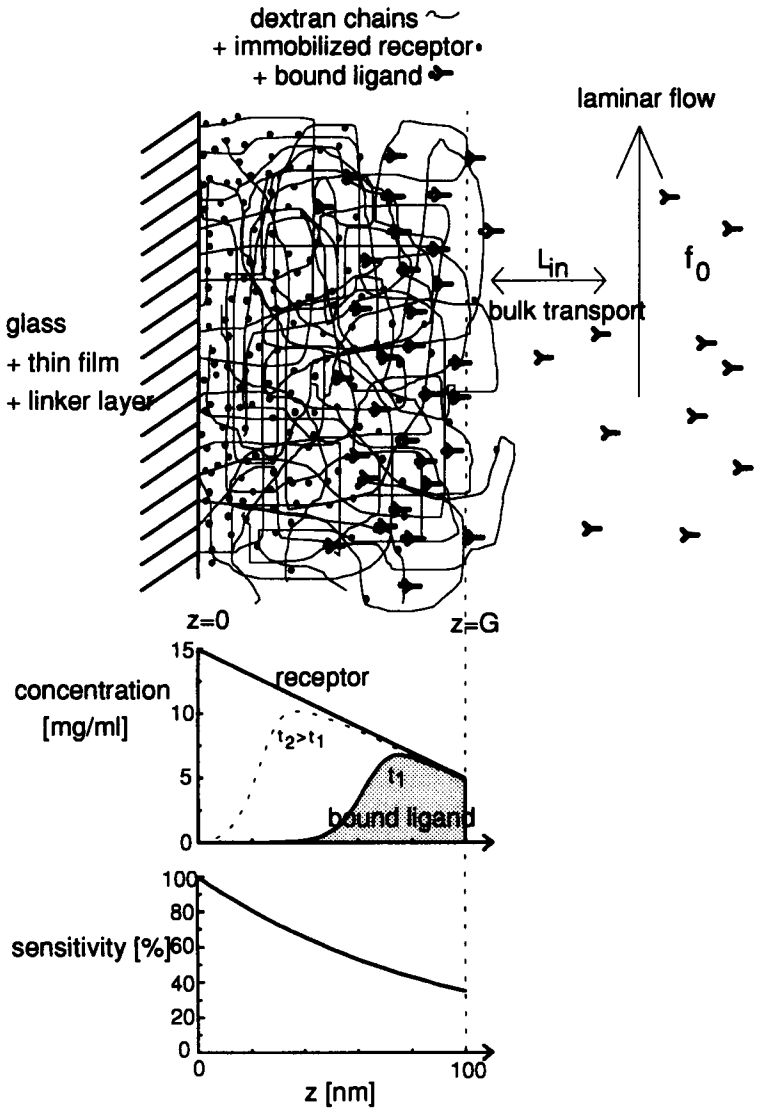

FIGURE 1 (*Upper graphics*) Schematic view of dextran chains with bound receptor and ligand flow. (*Middle plot*) Example for an assumed model receptor distribution $r(z)$ with a gel thickness of 100 nm and the calculated distributions of bound ligand $b(z, t)$. (*Lower plot*) Relative sensitivity distribution with σ = 95 nm.

following set of boundary and initial conditions has to be satisfied:

$$f(z, t = 0) = 0 \tag{2a}$$

$$\frac{\partial f}{\partial z}(z = 0, t) = 0 \tag{2b}$$

$$\frac{\partial f}{\partial t}(z = G, t) = k_{in}(f_0 - \gamma f(G, t)) - \frac{\partial b}{\partial t}(G, t), \tag{2c}$$

where f_o is the concentration of the bulk solution and k_{in} is a rate constant for material exchange between the gel and the bulk phase.

The numerical procedure to solve Eqs. 1 and 2 by discretization of the gel into layers (usually 50) of equal thickness Δz is described in the Appendix. To compare the result of the simulations with that of a two-compartment model (distinguishing only ligand inside and outside the gel matrix), only one layer with thickness G, obeying Eqs. 1b, 2a, and 2c (with γ = 1), was used.

The measured signal $R(t)$ of the evanescent wave biosensor is assumed to be proportional to the mass of ligand present in the gel, but the sensitivity is decaying exponentially:

$$R(t) = \int_0^G (f(z, t) + b(z, t))\alpha_0 e^{-z/\sigma} dz + \int_G^\infty f_0 \alpha_0 e^{-z/\sigma} dz. \tag{3}$$

For the calculations, a value of 95 nm (Liedberg et al., 1993) for the decay length σ was used, and the proportionality constant α_o was adjusted to give the same signal as in the ideal case of uniform receptor and sensitivity distribution. The constant small additive contribution of the bulk ligand to the signal was neglected. Because the BIACORE (the first commercially available instrument) was used to produce most of the published data, the present paper is adapted to the terminology of this literature. In the following, the signal as a function of time is called a "sensorgram," and it will be expressed in the resonance units (RU).

The transformation 1 RU = 1 pg bound protein/mm^2 (Stenberg et al., 1991; Karlsson et al., 1994) was used, which leads to 1 mg/ml = 100 RU for a gel of thickness 100 nm.

To estimate the influence of the receptor distribution in the gel, three different models were used: $r(z)$ was either constant within the gel, alternatively zero at the bottom of the gel (at $z = 0$), and linearly increasing toward the gel/bulk interface (at $z = G$), or zero at $z = G$ and linearly increasing toward $z = 0$. In the simulations, the receptor concentration will be expressed in units of its ligand-binding capacity. This will avoid complications due to different signal contributions of receptor and ligand caused by differences in their molar mass.

Because most of the parameters in Eqs. 1 and 2 are not known with accuracy and are dependent on a particular ligand, the influence of each parameter on the calculated sensorgram was analyzed in a series of simulations. The following estimates for their orders of magnitude were used:

a) The thickness of the gel, G, was assumed to be 100 nm (Löfås and Johnsson, 1990) unless otherwise specified.

b) The transport rate k_{in} was calculated through a transport coefficient L_{bulk}. The ligand flux, j, from the bulk into the first layer of the gel can be described by $j = L_{bulk}(f(G) - f_0)$. This flux increases the concentration of free ligand in the first layer by $j \cdot \Delta t/\Delta z$. Therefore, the rate constant k_{in} is given by $k_{in} = L_{bulk}/\Delta z$. In the BIACORE, the sensor is coupled to the bulk phase with a microfluidic cartridge. Correspondingly, L_{bulk} was assumed to be identical to the mass transport coefficient from the bulk to the boundary of a steady-state flow cell (Sjölander and Urbaniczky, 1991). This leads to

$$k_{in} \cong \frac{1}{\Delta z}\left(\frac{D_{bulk}{}^2 \nu}{h^2 b l}\right)^{1/3}, \tag{4}$$

where D_{bulk} denotes the diffusion coefficient of the ligand in the bulk, v the flow rate, h the height, b the width of the flow cell, and l the length of the active surface. This transport rate includes one major aspect of the flow outside the gel parallel to the sensor surface and the resulting ligand transport into the simulations. Obviously, it is dependent on the flow rate (in case of a stirred volume, it is dependent on the stirrer speed). In the simulations, unless otherwise specified a figure of $L_{bulk} = 5 \cdot 10^{-6}$ m/s was used (which resembles the value calculated assuming a bulk diffusion coefficient of $5 \cdot 10^{-11}$ m^2/s and a flow rate of 5 μl/min under the geometry of the flow-cell given in Karlsson et al., 1994).

c) Assuming a random-fiber model for the dextran and a spherical rigid ligand, the partition coefficient of the ligand into the gel can be calculated according to

$$K = e^{-\bar{A}h}, \tag{5}$$

where h denotes the chain length per unit volume and $\bar{A}$ the mean area of the projection of the ligand (Giddings et al., 1968). The dextran density is approximately 25 mg/ml (Karlsson et al., 1994). With a length increment of 5 Å per dextrose unit and assuming homogeneous spherical ligands with partial specific volume of 0.73 ml/g, Eq. 5 gives $K = \exp\{-6.38 \cdot 10^{-4}\ M^{2/3}\}$, that is, 0.25 for proteins of molar mass 100,000 or 0.15 for proteins (e.g., antibodies) with molar mass 160,000. The activity coefficient can be approximated by the reciprocal of K. It should be noted that the partition coefficient is exponentially dependent on the size of the ligand.

d) Many studies were performed on diffusion of tracer molecules in water:polymer mixtures. Theoretical considerations and experimental data lead to scaling laws of the form

$$D = D_0 e^{-\alpha c^\nu}, \tag{6}$$

where D_0 denotes the bulk diffusion coefficient and c the polymer concentration, with constants α and ν (Gorti and Ware, 1985; Phillies, 1985; Langevin and Rondelez, 1978). To estimate the diffusion coefficient in the gel, the dextran matrix with immobilized and at least partially liganded receptor should be taken into account. At an immobilization level of 1000 RU (~10 mg/ml) and assuming a comparable molar mass of ligand and receptor, a typical value for the matrix density is 40–50 mg/ml (although this value is often largely exceeded in the literature). Comparisons with experimental data and constants given for different tracer particles and polymer solutions (Gorti and Ware, 1985; Phillies, 1985; Langevin and Rondelez, 1978) support that the diffusion coefficient inside the gel is diminished roughly by a factor of 10–20. Therefore, a value of 10^{-12} m^2/s for the diffusion coefficient in the dextran matrix was used. However, because this estimate is uncertain, it was varied in different simulations and the influence of this parameter will be described below. It should be noted that the values of the constants α and ν in Eq. 6 given in the literature differ considerably for different systems, depending on the size of the ligand and on its electrostatic interaction with the polymer, i.e., on the buffer composition (Gorti and Ware, 1985). This is of particular interest because the carboxylated dextran has a net negative charge, with which many proteins possibly interact, resulting in lower diffusion coefficients. Some experimental evidence in the biosensor literature for protein/dextran interaction can be found in (Zahn et al., 1994; Takano et al., 1994; Cooper et al., 1994).

RESULTS

Distribution of free and bound ligand in the gel during the association phase

In general, at low chemical on rate and off rate constants k_+ and k_-, the ideal binding progress curve (as described in the Appendix) was observed. With the parameter values given above, in the absence of any receptor, the ligand was equilibrated in the gel in less than 0.1 s. In the presence of immobilized receptor, this process is slower. The governing factor for this retardation is $k_+ r$, the product of chemical on rate and concentration of immobilized receptor, since $k_+ r \Delta z$

describes the reaction flux density in each layer in the initial phase of binding. To make the distinction of the different transport-related phenomena and a comparison with literature values easier, in the following the regimes of k_+r will be additionally expressed in terms of a corresponding chemical on rate k_+^* for 2500 RU total ligand binding capacity of the receptor and a ligand molar mass of 50,000. Clearly, for different cases these values must be adjusted according to

$$k_+^{**} = k_+^* \cdot \frac{\text{Mw}}{50{,}000} \cdot \frac{2500\ \text{RU}}{\text{Binding capacity}}.$$

It was found that the influence of binding on the transport within the gel can be neglected, if $k_+r \leq 100$ RU(mg/ml)$^{-1}$s^{-1} ($k_+^* \leq 2 \cdot 10^3$ M^{-1}s^{-1}). In this case the free ligand in the matrix is equilibrated in less than 1 s with vanishing concentration gradient of the bound ligand. For all faster reactions nonuniform concentration distributions of both free and bound ligand were observed, which persist for the entire time course of the binding until equilibrium is reached. However, for only moderately transport limited reactions, the gradient of bound material does not change significantly during most of the binding phase (Fig. 2). In this range of reaction rates, the two-compartment model produces approximately the same results.

A totally different behavior of $f(z, t)$ and $b(z, t)$ is found in highly transport limited cases $k_+r \geq 10^5$ RU(mg/ml)$^{-1}$ s^{-1} ($k_+^* \geq 2 \cdot 10^6$ M^{-1}s^{-1}) at a final receptor saturation exceeding 90%. The bound ligand propagates into the gel in the form of an inward moving front of saturation (Fig. 3 *B*). It extends from receptors with almost the final plateau equilibrium binding level at the gel/bulk interface, to the inner portions of the gel, where still almost no ligand is bound. The inflection point of the front is moving with time and indicates the region of the gel where the local binding reaction is the fastest. The width of the front of this "traveling saturation binding" is mainly dependent on the degree of final receptor saturation and the product k_+r. It can reach a few nanometers or less for very high k_+r. In the limit of infinitely fast and irreversible reactions, for which an analytical description of the binding is given in the Appendix, it degenerates to a rectangular shape (Eq. A13). The position of the saturation boundary in exclusively transport limited cases (Eq. A12) coincides within a few nanometers with the inflection points in Fig. 3 *B*.

The sensorgram: effect of the exponentially decaying sensitivity

To illustrate the relationship between the measured sensorgram and the distributions $b(z, t)$, the gel was divided into three regions of equal size. The time course of binding $b(z, t)$ was calculated, and by Eq. 3 the contribution of each region to the signal $R(t) = R_1(t) + R_2(t) + R_3(t)$ was determined.

For slow reactions, where the transport influence is negligible, all regions in the gel contribute in a similar way to the signal. In this ideal case, $R_1(t)$, $R_2(t)$, and $R_3(t)$ are proportional. The contribution of the region at $z = G$ is lowest, reflecting the decaying sensitivity in the gel. However, with increasing binding rates they exhibit differences in the shape. Fig. 4 *A* shows the slight loss of proportionality between the signals of the regions for the binding phase shown in Fig. 2. However, a two-compartment model as an approximation is suitable. At still higher binding rates and high saturation, qualitative differences occur (Fig. 4 *B*): The region near the bulk, $R_1(t)$, reaches its plateau value relatively rapidly, whereas the regions more distant from the bulk and closer to the solid surface experience a time delay in their binding curves. In addition, the latter signal, $R_3(t)$, is the strongest, and consequently the derivative dR_3/dt is highest. Therefore, the sensorgram exhibits an increasing slope.

This phenomenon can also be found in the pure transport-determined model (see Appendix). The sensorgram is dependent on the velocity of the moving boundary and the decay constant of the sensitivity ($dR/dt = dR/dB \cdot dB/dt$, where $B(t)$ denotes the position of the boundary).

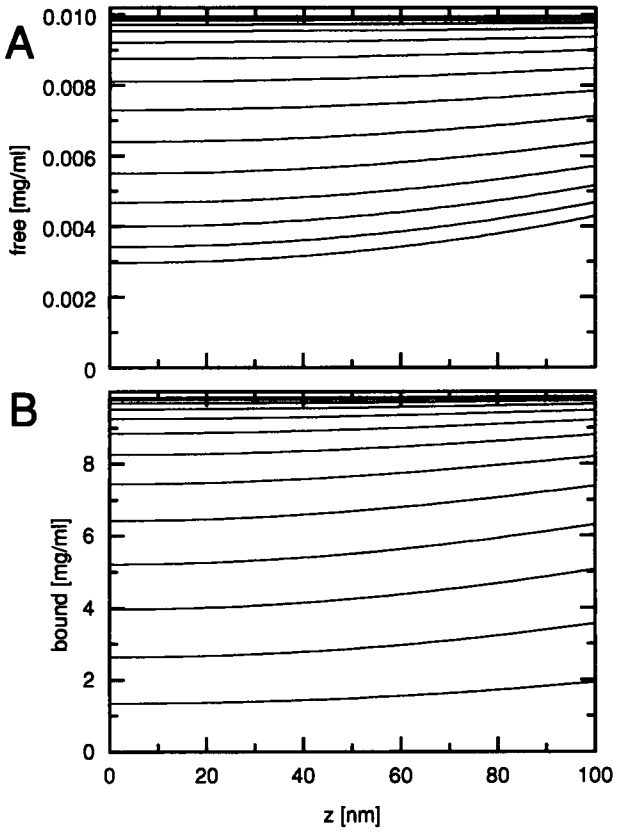

FIGURE 2 Calculated distributions of (*A*) free ligand $f(z, t)$ and (*B*) bound ligand $b(z, t)$ in the association phase of a moderately transport limited reaction in time intervals of 5 s. Simulation parameters: chemical on rate $k_+ = 10$(ml/mg)$^{-1}$·s^{-1}; off rate $k = 10^{-3}$ s^{-1}; bulk ligand concentration $f_0 = 0.01$ mg/ml; concentration of homogeneous immobilized receptor $r = 1000$ RU; partition coefficient $K = 1$; diffusion coefficient $D = 10^{-12}$ m^2/s; transport coefficient $L_{\text{bulk}} = 5 \cdot 10^{-6}$ m/s; thickness of the gel G = 100 nm.

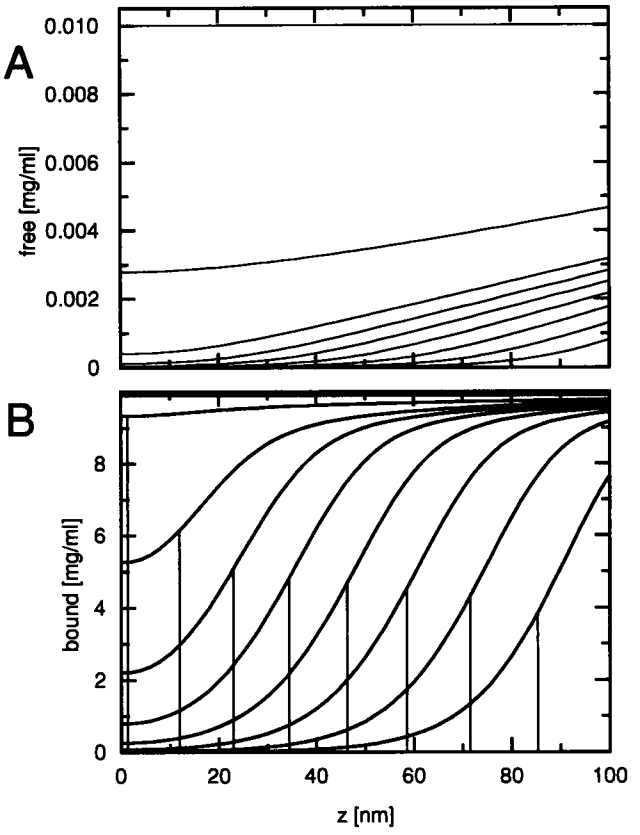

FIGURE 3 Calculated distributions of (*A*) free ligand $f(z, t)$ and (*B*) bound ligand $b(z, t)$ in the association phase of a highly transport limited reaction in time intervals of 3 s. Simulation parameters: chemical on rate $k_+ = 10^3(\text{ml/mg})^{-1}\cdot\text{s}^{-1}$, off rate $k_- = 0.1\ \text{s}^{-1}$, all other parameters are the same as in Fig. 2. The vertical lines indicate the *z*-position of the boundary $B(t)$ for an irreversible exclusively transport controlled model (Eq. A12) for the same time intervals.

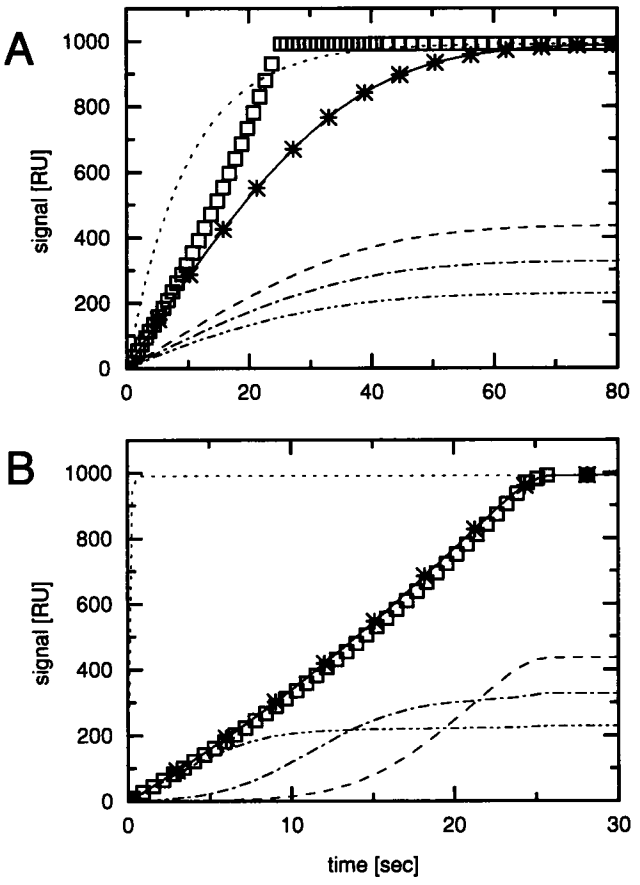

FIGURE 4 Effect of inhomogeneities in the ligand distribution and in the sensitivity distribution on the signal. The signal (——) is decomposed in the contributions of the part of the gel $0 < z \leq 33$ nm (– – –), 33 nm $< z \leq 66$ nm (– · –), and 66 nm $< z \leq 100$ nm (– ·· –). For comparison, the ideal binding progress curve (···) and the infinite fast irreversible binding model (□) are shown. Stars (*) indicate the signal at the time intervals of Figs. 2 and 3, respectively. Sensitivity decay constant σ is 95 nm. Simulated sensorgram with parameters as in Figs. 2 *A* and 3 *B*, respectively.

These two factors change their relative magnitudes with time. First, the decrease in the boundary velocity ($dB/dt \propto 1/(G - B)$) compensates for the increase of sensitivity ($dR/dB \propto e^{(G-B)/\sigma}$). Then, the exponential governs the sensorgram, producing the increasing slope. It can be shown analytically that this effect is more pronounced with increasing ratio G/σ. It is obvious that dR/dB is sensitive to the details of the optical setup and that dB/dt will be determined by the receptor distribution. Therefore, these factors will influence the sensorgram (see Fig. 5). The resemblance of the simulated sensorgram in Fig. 4 *B* to that of an exclusively transport-controlled binding (*open square*) shows that, for the parameter values used in the simulation of Fig. 3, a moving rectangular boundary as described in the Appendix is a reasonable model. A two-compartment model is not sufficient.

Dependence of the sensorgram on chemical on and off rates

Simulations were performed with different chemical on rates, keeping the equilibrium constants $K_d = k_-/k_+$ constant in each set. The simulated sensorgrams can be divided into two groups, depending on the final receptor saturation. In the following, typical results are described.

Fig. 6 shows the calculated sensorgrams at high final receptor saturation (99%) ($K_d = 10^{-4}$ mg/ml, $c_o = 0.01$ mg/ml, $r = 1000$ RU). In Fig. 6 *B* the signal is plotted versus a normalized time, which is scaled for each curve by the on rate. Without transport limitations, in this plot all curves would be expected to coincide with the ideal binding progress curve (*circles*). In Fig. 6 *A* the time scale is unchanged. Beginning with $k_+r \geq 100$ RU$(\text{mg/ml})^{-1}\text{s}^{-1}$ ($k_+^* \geq 2 \cdot 10^3\ \text{M}^{-1}\text{s}^{-1}$) increasing deviations from the idealized binding process can be observed. Above 10^5 RU$(\text{mg/ml})^{-1}\text{s}^{-1}$ ($k_+^* \geq 2 \cdot 10^6\ \text{M}^{-1}\text{s}^{-1}$) no substantial decrease in the time to reach the plateau value of the sensorgram can be achieved. Instead, a deformation into a sigmoidal-shaped sensorgram takes place that is a consequence of the moving binding front discussed above (Fig. 3). All on

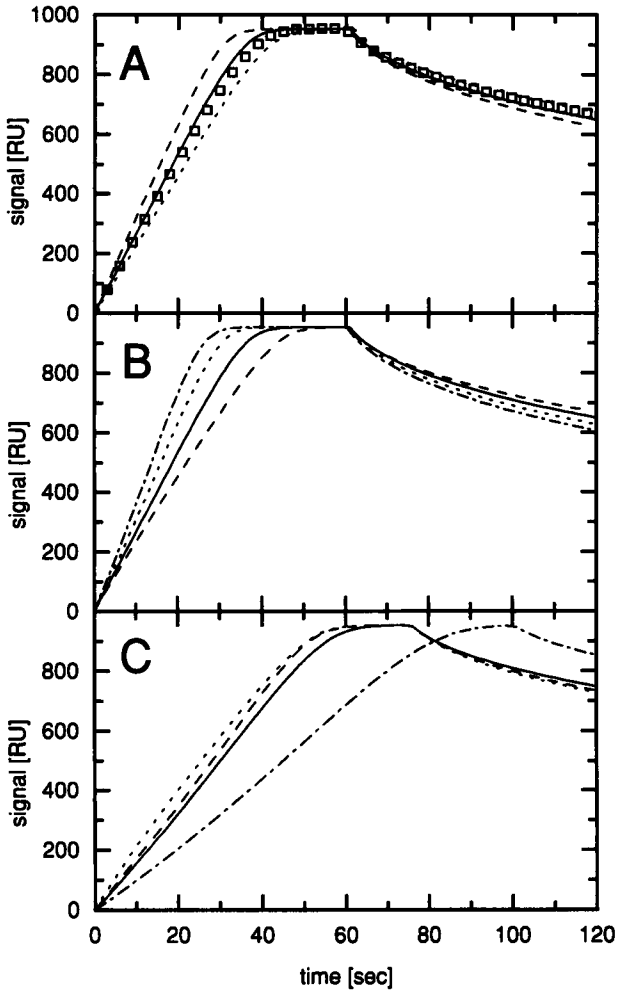

FIGURE 5 Sensitivity of the simulated sensorgram to several parameters unrelated to chemical reaction rate. Unless indicated otherwise r = 1000 RU (uniform), $k_+ = 100$ (ml/mg)$^{-1}$·s^{-1}, $k_- = 0.05$ s^{-1}, $f_0 = 0.01$ mg/ml, $K = 0.3$, $D = 10^{-12}$ m^2/s, $L_{bulk} = 5 \cdot 10^{-6}$ m/s, $G = 100$ nm, and $\sigma = 95$ nm. (*A*) Influence of the receptor distribution at constant total binding capacity of 1000 RU: uniform (——), linearly increasing (– – –), and decreasing (···) toward bulk. The sensorgram calculated in a two-compartment model (□) (with L adjusted to achieve a unchanged transport rate (Eq. A20)) corresponds best to a receptor distribution $r(z) = R_o\delta(z - z^*)$ at a point z^* within the gel. (*B*) Variation of the partition coefficient K = 1 (– · –), $K = 0.5$ (···), $K = 0.3$ (——), and $K = 0.2$ (– – –). (*C*) Effect of a reduction of the transport parameters: $L_{bulk} = 2.5 \cdot 10^{-6}$ m/s (——); $L_{bulk} = 1.5 \cdot 10^{-6}$ m/s (– · –); $D = 5 \cdot 10^{-13}$ m^2/s (···), and effect of different decay length $\sigma = 60$ nm with $D = 5 \cdot 10^{-13}$ m^2/s (– – –).

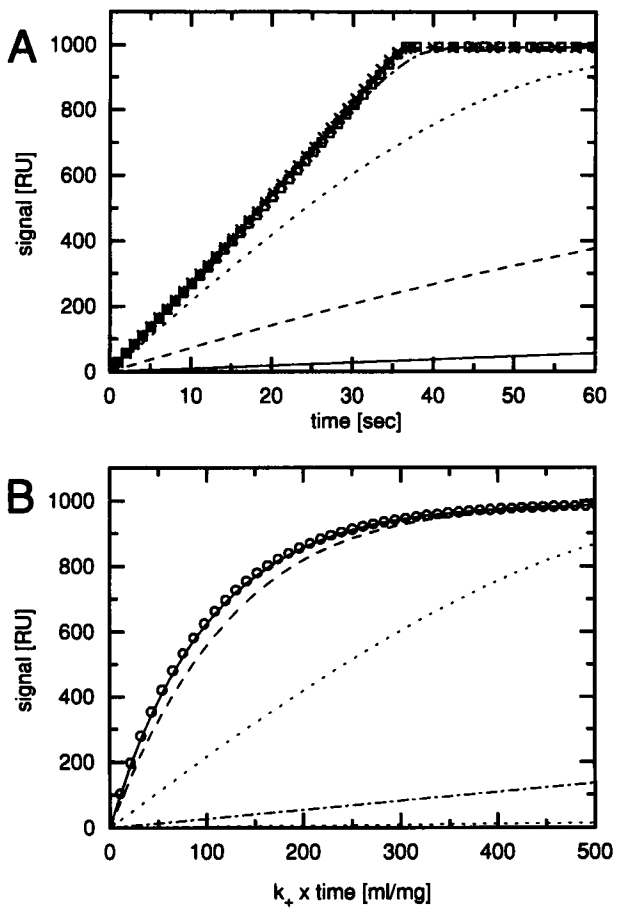

FIGURE 6 Influence of mass transport at high receptor saturation. (*A*) Simulated sensorgrams of the association phase for $K_d = 10^{-4}$ mg/ml, f_0 = 0.01 mg/ml, $r = 1000$ RU, $K = 0.3$, $D = 10^{-12}$ m^2/s, $L_{bulk} = 5 \cdot 10^{-6}$ m/s, $G = 100$ nm, $\sigma = 95$ nm. Chemical on rates k_+: 0.1 (——), 1 (– – –), 10 (···), 100 (– · –), 1000 (–×–), and 10,000 (ml/mg)$^{-1}$·s^{-1} (–+–). Infinitely fast irreversible binding model (□). (*B*) Same sensorgrams plotted signal versus time * k_+ with ideal binding progress curve (○).

rates $k_+r \geq 10^7$ RU(mg/ml)$^{-1}$s^{-1} ($k_+^* \geq 2 \cdot 10^7$ M^{-1}s^{-1}) produce the same sigmoidal sensorgram. The two-compartment model is appropriate only up to $k_+r \approx 10^4$ RU(mg/ml)$^{-1}$s^{-1} ($k_+^* \geq 2 \cdot 10^5$ M^{-1}s^{-1}).

At low final receptor saturation only small concentration gradients in $b(z, t)$ and no increasing slope of the sensorgram was observed. A two-compartment model describes the qualitative aspects well. Deviations from the ideal sensorgram were found to begin at $k_+r \geq 100$ RU(mg/ml)$^{-1}$ s^{-1} ($k_+^* \geq 2 \cdot 10^3$ M^{-1}s^{-1}), and the limit in which the sensorgram is independent of the on rate was at approximately 10^5 RU(mg/ml)$^{-1}$s^{-1} ($k_+^* \approx 2 \cdot 10^6$ M^{-1}s^{-1}) (Fig. 7).

Effects of ligand and receptor concentration

In a pseudo-first-order reaction a decrease in the concentration of ligand results in a slower binding process. But because the diffusional fluxes decrease by the same amount, no changes in the diffusion influence can be observed. The calculated sensorgrams are identical to those of a binding with higher chemical off rate, measured on a slower time scale. This relationship between sensorgrams is based on the structure of Eq. 1 and was verified in the simulations. Therefore, the form of the plots in Figs. 6 and 7 remain unchanged for lower ligand concentrations, if the time scale is appropriately normalized. The symmetries of the contributions of reaction and diffusion to the total time course of the sensorgram indicated in Eq. 1 imply that the occurrence

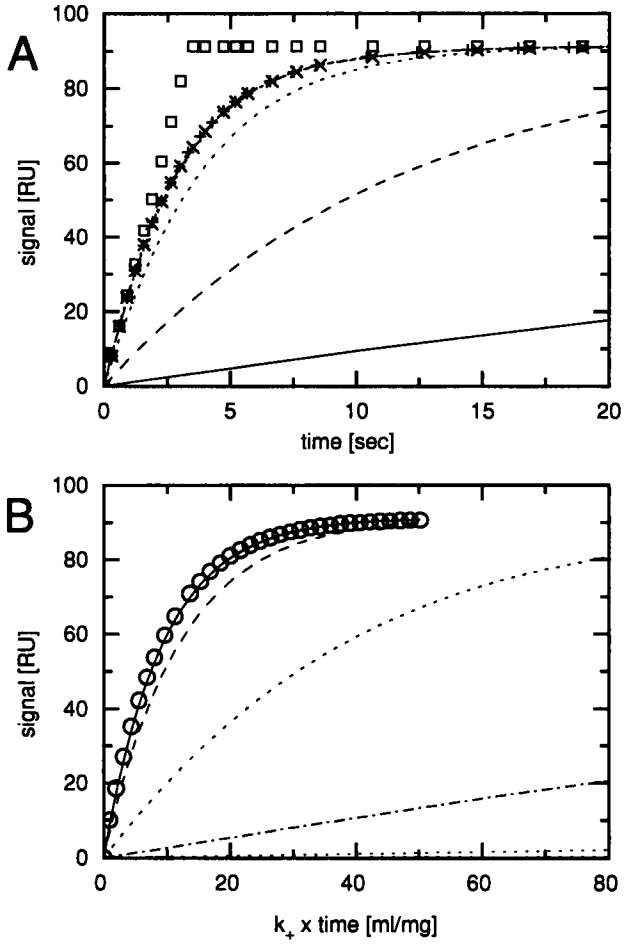

FIGURE 7 Influence of mass transport at low receptor saturation. (*A*) Simulated sensorgrams of the association phase for K_d = 0.1 mg/ml, f_0 = 0.01 mg/ml, r = 1000 RU, K = 0.3, $D = 10^{-12}$ m^2/s, $L_{bulk} = 5 \cdot 10^{-6}$ m/s, G = 100 nm, σ = 95 nm. Chemical on rates k_+: 0.1 (——), 1 (– – –), 10 (···), 100 (– · –), 1000 (–×–), and 10,000 (ml/mg)$^{-1}$·s^{-1} (–+–). Infinitely fast irreversible binding model (□). (*B*) Same sensorgrams plotted signal versus time * k_+ with ideal binding progress curve (○).

of inhomogeneities is in principle not restricted to short time intervals after the injection of the ligand.

Experimentally, the decrease of the ligand concentration in the bulk does not seem to have an advantage, because the mass transport influences apparently remain unchanged (Glaser, 1993; Karlsson et al., 1994). On the other hand, a lower ligand concentration may permit the detection of binding in a better time resolution. But higher ligand concentrations (and higher saturations) have the advantage of producing deviations from apparent ideal sensorgrams and can signal diffusion-limited cases.

A different situation occurs with the reduction of the amount of immobilized receptor. This leads to a reduced binding flux and therefore to a faster transport of the ligand. Again, the sensorgrams of reduced receptor concentrations are closely related to those shown in Figs 6 and 7. They are equivalent to sensorgrams of processes with proportionally lower chemical on rate at higher ligand concentration, measured with lower sensitivity. Therefore, the diffusional influences are reduced. As pointed out before (Glaser, 1993; Karlsson et al., 1994), this technique permits extension of the dynamical range of the instrument, unfortunately limited by the signal-to-noise ratio of the instrument.

Calculations were performed with three different models of receptor distribution in the gel (see above). If the immobilized receptor is distributed nonuniformly in the gel, the change in the signal compared to a uniform distribution is dependent on the final average receptor saturation and the reaction rate. For a low saturation the influence of the receptor distribution is negligible. In contrast, at high average receptor saturation it begins to influence the sensorgram significantly at $k_+r \geq 10^4$ RU(mg/ml)$^{-1}$s^{-1} ($k_+^* \geq 2 \cdot 10^5$ M^{-1}s^{-1}) (Fig. 5). To estimate the potential influence of the receptor distribution on the moving front of saturation $B(t)$ in exclusively transport determined cases, Eq. A10 was integrated with the linear decreasing or increasing receptor model. The time required to saturate the receptors is altered by ±35% (faster binding with more receptor near the bulk). If the receptor is linearly increasing from the gel/bulk interface to the sensor surface, the effect on the sensorgram is similar to those of reduced partition or diffusion coefficient.

Influence of transport coefficient, diffusion coefficient, and partition coefficient

Both the diffusion coefficient inside the gel and the transport coefficient into the gel govern the onset of mass transport-influenced binding. With the parameter values used in the simulations, their effects are approximately of equal magnitude. This is true independently of the receptor saturation at equilibrium.

In simulations with varying transport coefficients from bulk to gel, the onset of deviations from ideality is found at slightly higher k_+r if the transport coefficient is increased (corresponding to the use of a higher flow rate in the experiment). At high reaction rates, the shape of the sensorgrams was nearly independent of the transport coefficients, which modulate primarily their time scale (see Fig. 5). In addition, the limit of chemical on rates for which the sensorgram is exclusively transport limited was not changed. Generally, the influence of the transport from bulk to gel is decreasing with decreasing diffusion and partition coefficient (then the transport within the matrix becomes the limiting factor).

Because the diffusion coefficient determines the distribution of ligand in the gel, it also determines the regimes of kinetic rate constants for which the described effects of inhomogeneity can be observed. A lower diffusion coefficient produces the same relative deviations from an ideal sensorgram as proportionally higher reaction rate constants (and simultaneously with a higher transport coefficient from the bulk to the gel). With lower diffusion coefficients, traveling saturation binding may be observed at lower final receptor saturation and lower reaction rates.

In the simulations, a change of the partition coefficient produced the same results as changes in the diffusion coefficient. With a partition coefficient lower than unity, the gradients in $f(z, t)$ (Figs. 2 *A* and 3 *A*) become smaller and the transport slower. As a consequence the influence of diffusion within the gel on the sensorgram increases. It takes a longer overall time to reach equilibrium, and $b(z, t)$ exhibits a more pronounced traveling saturation binding.

Although in general, diffusion within the gel and transport from bulk to gel both determine the overall transport rate, the two effects differ initially. In cases where Eq. A10 is a good approximation, initially only L_{bulk} determines the sensorgram. This changes when the boundary is at a position z^*, where $(G - z^*)/DK$ is comparable to $1/L_{bulk}$. This effect produces an initial shoulder, i.e., a higher initial slope, which is soon followed by a phase of lower, approximately constant slope (Fig. 8). As can be seen in Fig. 8 the initial shoulder can introduce an error in the estimation of the baseline after the buffer change (with possible refractive index change), which amounts in this case to 5–10% of the equilibrium plateau level.

Dissociation phase

During the dissociation phase, nearly vanishing concentration gradients of bound ligand were observed under all conditions. No process similar to the traveling saturation boundary in the association phase was found. Inspection of Eq. 1b shows that the cause of nonideality during the dissociation is a nonzero free ligand concentration in the gel. This produces rebinding to the receptor, also known as the retention effect (Silhavy et al., 1975). Therefore, the deviations again are dependent on k_+r. Fig. 9 shows the increasing deviations from ideality caused by transport limitation with higher on rates. In Fig. 9 *B* the time is scaled by the off rate and the curves again should be identical for negligible transport influence. It is evident that the limits for the onset of deviation as well as for the total independence from reaction rates are the same as in the association phase.

Because the concentration gradients of free ligand in the gel are very small when receptor is initially at equilibrium with free ligand, a two-compartment model might be considered as a reasonable model for the dissociation phase. On the other hand, as evident from the dissociation phase of the simulated sensorgrams plotted in Fig. 5, the receptor distribution in the gel, the decay length of the sensitivity, the diffusion coefficient, and the partition coefficient all have serious effects on the signal during the dissociation phase.

However, the two-compartment model is not adequate when the dissociation phase starts from an incomplete association phase that is characterized by traveling saturation

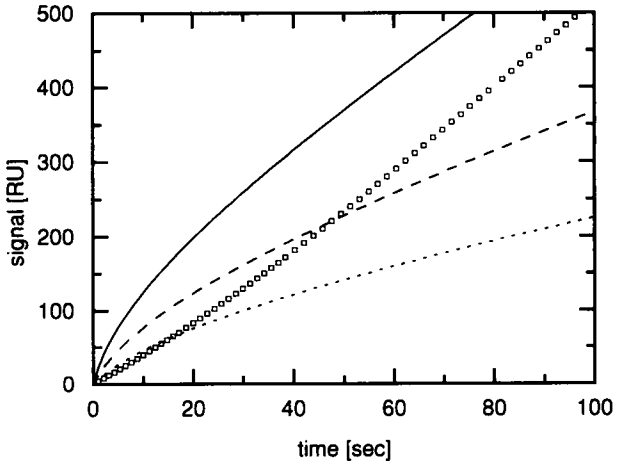

FIGURE 8 Characteristic initial shoulder produced by low diffusion coefficient. Sensorgram with different ligand concentrations: f_0 = 0.01 mg/ml (——), 0.005 mg/ml (– – –), and 0.0025 mg/ml (···) with K = 0.3, $D = 10^{-13}$ m²/s (a factor of 10 lower than other simulations), $L_{bulk} = 5 \cdot 10^{-6}$ m/s, $k_+ = 10^3$ (mg/ml)$^{-1}$·s^{-1}, $k_- = 0.1$ s^{-1}, σ = 95 nm, r = 1000 RU. Sensorgram with equal overall transport coefficient (in the steady-state model of Eq. A20), but with high diffusion coefficient (10^{-11} m²/s) and correspondingly lower bulk/gel transport coefficient ($L_{bulk} = 5.4 \cdot 10^{-7}$ m/s) (□) .

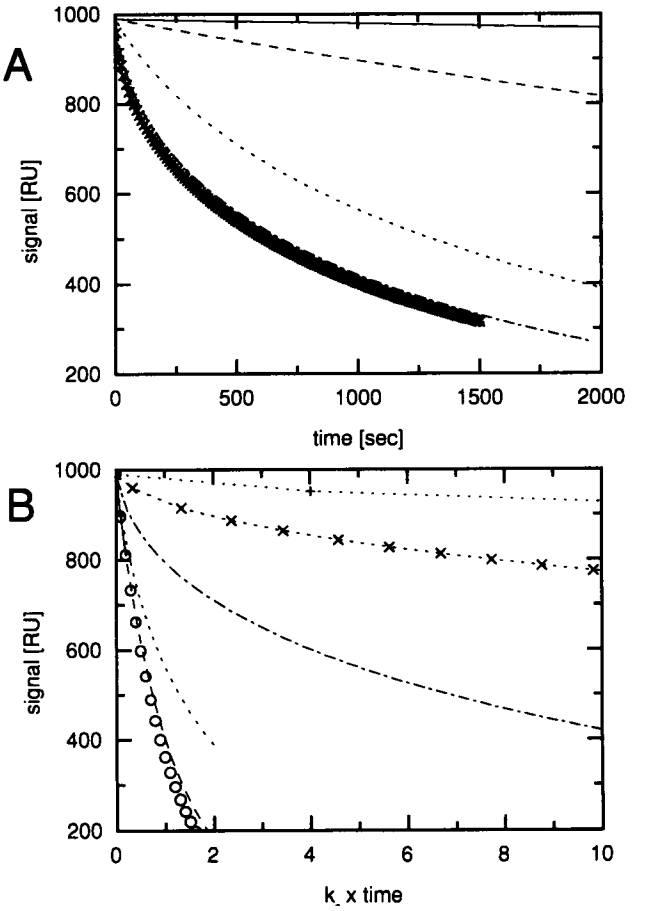

FIGURE 9 (*Upper plot*) Dissociation phase of simulated sensorgrams for constant equilibrium constant $K_d = 10^{-4}$ mg/ml at different chemical on rates k_+: 0.1 (——), 1 (– – –), 10 (···), 100 (– · –), 1000 (–×–), and 10,000 (mg/ml)$^{-1}$·s^{-1} (–+–). Parameters: f_0 = 0.01 mg/ml, r = 1000 RU, K = 0.3, $D = 10^{-12}$ m²/s, $L_{bulk} = 5 \cdot 10^{-6}$ m/s, G = 100 nm, σ = 95 nm. (*Lower plot*) Same sensorgrams plotted signal versus time * k_- and ideal binding progress curve (○).

binding (at high on rates and high saturation). If the interruption of the association phase is made at approximately two-thirds of the plateau signal, the traveling shoulder is relatively close to the sensor surface. The change from association to dissociation starts two processes. First, it causes the regions of the gel near the gel/bulk interface to release some of the ligand. Second, near the inner sensor surface diffusive rearrangement and equilibration of the shoulder take place. This rearrangement near the sensor surface transports part of the ligand to positions with higher sensitivity in the gel. Altogether, because the boundary was stopped in the steep part of the exponential sensitivity decay, the signal increase in that region can match the ligand loss near the more insensitive gel/bulk interface, and a slight initial increase in the signal can occur (Fig. 10). This increase is very small and could be difficult to detect experimentally because of noise and baseline drifts, but there are hints in the literature that such an effect exists (e.g., Gershon and Khilko, 1995).

Effects of the gel thickness

When the gel size is varied at constant total amount of immobilized receptor, the contribution of the diffusion within the gel to the overall transport is directly modulated. The increase of the gel thickness has approximately the same effect on the sensorgrams as a proportional lowering of both the diffusion coefficient and the sensitivity decay length. Therefore, with a smaller gel, fewer inhomogeneities occur in the gel, and traveling saturation binding can be found only at higher reaction rates. Furthermore, increasing the flow rate in the bulk is more effective in reducing the transport influence. In contrast to the results for a 100-nm-thick gel, a gel of 10 nm thickness was found to be nearly insensitive to the receptor distribution (using the diffusion and partition coefficient outlined above). Conversely, at the higher thickness all deviations from ideal binding progress curves related to the diffusion in the gel matrix (e.g., the initial shoulders, apparent cooperative binding profile) are more pronounced, as evident in Fig. 11. These differences in the sensorgrams due to different size of the gel matrix are increasing with lower diffusion and partition coefficient of the ligand.

The residual transport influence in the sensorgram calculated for a 10-nm gel in Fig. 11 can be further reduced by an increased diffusion and partition coefficient, corresponding to a smaller dextran density. However, the limiting factor under these conditions is the external transport from the bulk flow to the bulk/gel interface.

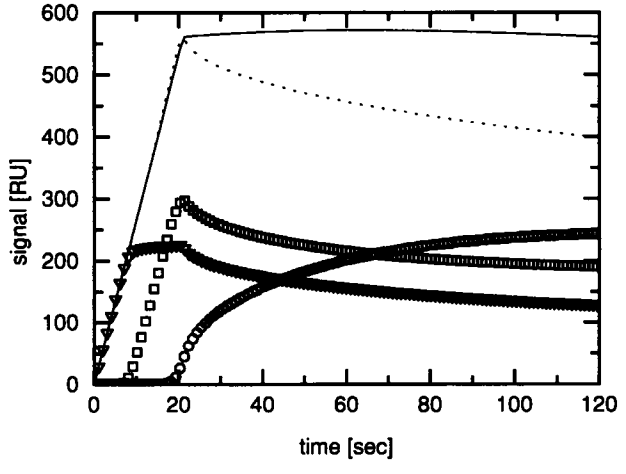

FIGURE 10 Effect of incomplete association on the dissociation profile. (——) Calculated sensorgram with 1000 RU receptor, interrupted association after ~2/3 saturation. Included are the signal contributions of the gel regions $0 < z \leq 33$ nm (○), $33 < z \leq 66$ nm (□), and $z > 66$ nm (▽). For comparison: sensorgram after nearly complete saturation of 565 RU (···). Other parameters are the same in both sensorgrams: $K = 0.3$, $D = 10^{-12}$ m^2/s, $L_{bulk} = 5 \cdot 10^{-6}$ m/s, $k_+ = 10^4$ (mg/ml)$^{-1}$·s^{-1}, $k_- = 1 \cdot s^{-1}$, $\sigma = 95$ nm, $f_0 = 0.01$ mg/ml.

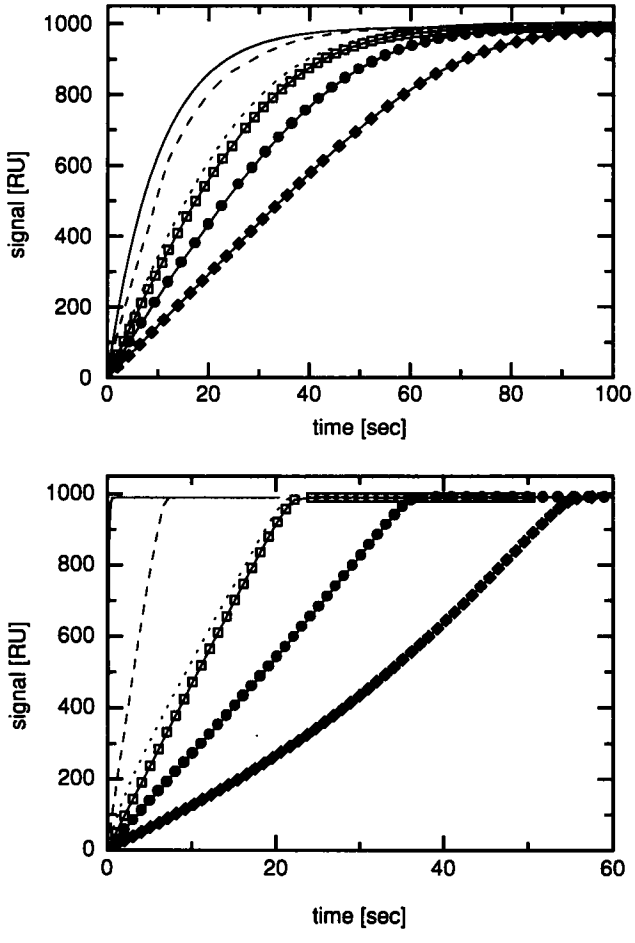

FIGURE 11 Effect of the thickness of the gel matrix on the sensorgram (with unchanged total amount of receptor). Parameters: $k_+ = 10$ (mg/ml)$^{-1}$·s^{-1} (*upper plot*); $k_+ = 1000$ (mg/ml)$^{-1}$·s^{-1} (*lower plot*); $K_d = 10^{-4}$ mg/ml; $f_0 = 0.01$ mg/ml; $r = 1000$ RU; $K = 0.3$; $D = 10^{-12}$ m^2/s; $L = 5 \cdot 10^{-6}$ m/s; $G = 10$ nm (□); $G = 100$ nm (●); $G = 220$ nm (◆). Sensorgram with high external flow ($L_{bulk} = 5 \cdot 10^{-5}$ m/s) $G = 10$ nm (– – –), $G = 100$ nm (···), and the ideal binding progress curve (——) are included.

Fitting the sensorgrams with exponentials

Most of the simulated sensorgrams can be empirically fitted by an ideal binding progress curve, as it is described in the Appendix, neglecting mass transport (Fig. 12). However, in many cases the apparent rate constants k_+^{app} and k_-^{app} deviate substantially from the true reaction rate constants k_+ and k_-(Fig. 13), even though the deviation of the best-fit model from the simulated data was <1%, i.e., within experimental uncertainty.

In the association phase, when $k_+r \geq 10^4$ RU(mg/ml)$^{-1}$s^{-1} ($k_+^* \geq 2 \cdot 10^5$ M$^{-1}s^{-1}$) at high final saturation, significant deviations from the ideal exponential saturation were observed. These sensorgrams generally could not be fitted by single or multiple exponentials (with physically meaningful coefficients) because they contain a linear initial binding phase. However, a different behavior is found if the receptor distribution is confined mainly to the surface of the gel with a low receptor concentration within the gel. In this case a low diffusion and partition coefficient of the ligand leads to double exponential association phases for $k_+r \geq 10^3$ RU(mg/ml)$^{-1}$s^{-1} ($k_+^* \geq 2 \cdot 10^4$ M^{-1}s^{-1}). The faster binding phase corresponds to the binding at the gel surface, the slower corresponds to the binding to the receptor within the gel, which is subject to retardation due to the additional transport. Both apparent rate constants are still significantly lower than the true reaction rate.

In the dissociation phase, for $k_+r \geq 10^4$ RU(mg/ml)$^{-1}$ s^{-1} ($k_+^* \geq 2 \cdot 10^5$M^{-1}s^{-1}) double exponential decay was found (Fig. 12). The fast decay component was more pronounced (higher relative amplitude) with higher reaction rates, although the apparent fast off rate was at high on rates generally still significantly lower than the true off rate. This is especially true if a part of the initial data is discarded, as is necessary in a real experiment because of artifacts of the buffer change. The fit could typically be improved by a baseline offset (deviations of <0.5%). When the dissociation kinetics was entirely transport limited, and the dissociation phase was observed until the decay proceeded to 5% of the plateau value, a third exponential could lead to a fit with an extremely high accuracy (data not shown).

For the cases where a compartment model is reasonable, estimates for the reduction of the apparent binding rates can be derived on the basis of steady-state approximations, as shown for example by DeLisi (1980) and Glaser (1993). In the Appendix, steady-state conditions for the consecutive transport in the bulk, transport within the gel, and reversible binding reaction are described. The following assumptions are used: 1) The transport distance of the ligand within the gel is $G/2$; 2) At the surface the concentration of the ligand is reduced by the factor K (partition coefficient); and 3) the chemical on rate is enhanced by the factor $\gamma = K^{-1}$ (activity coefficient). This leads to the ratio of apparent chemical reaction rates to the true rates

$$\frac{k_+^{app}}{k_+} = \frac{k_-^{app}}{k_-} = \frac{1}{1 + k_+(r-b)G\dfrac{2DK + GL_{bulk}}{2DKL_{bulk}}}. \quad (7)$$

A combined effective transport rate can be expressed as

$$k_{tr} = \frac{2DKL_{bulk}}{G(2DK + GL_{bulk})}. \quad (8)$$

Fig. 13 shows the apparent rate constants as a function of the true rates for the sensorgrams in Figs. 6, 7, and 9 that could be fitted with single exponentials. It is evident that for these cases, Eq. 7 (Fig. 13, *solid line*, where $b = r/2$ is assumed) gives a reasonable estimate for the effect of transport limitation. In turn, for the interpretation of experimental data, the appearance of deviations from apparently mono-exponential binding (e.g., double exponential dissociation), could indicate—if the origin is transport limitation—that basically only transport rates were measured, with differences from the measured to the true rate constant of possibly a factor of 10 or more. This shows that it is essential to use experimental techniques to rule out mass transport as the origin of these effects. Methods to extract information about the reaction rates in transport-influenced sensorgrams are discussed by Schuck (manuscript submitted for publication).

According to the simulations, in the case of low receptor saturation no deviation from the form of an ideal exponential binding progress curve will be detected, even for very high reaction rates ($k_+(r-b)/k_{tr} \gg 1$). In this limit of very high reaction rates, the measured k_+^{app} and k_-^{app} become independent of the reaction rates:

$$k_{+,lim}^{app} = \frac{k_{tr}}{r-b}$$
$$k_{-,lim}^{app} = K_d\frac{k_{tr}}{r-b}. \quad (9)$$

These rate constants $k_{+,lim}^{app}$ and $k_{-,lim}^{app}$ represent the fastest apparent rates that can be measured. The association phase contains only information about the transport, whereas the dissociation phase also depends upon the equilibrium constant. With Eq. 8, and the diffusion coefficient, partition coefficient, gel thickness, and the external transport coefficient as given above (assuming half receptor saturation), typical values are

$$k_{+,lim}^{app} \approx 5 \cdot 10^3\frac{\text{Ligand molar mass}}{\text{Binding capacity / RU}}\text{M}^{-1}\text{s}^{-1}$$
$$k_{-,lim}^{app} \approx 5 \cdot 10^3 \cdot K_d \cdot \frac{\text{Ligand molar mass}}{\text{Binding capacity / RU}}\text{M}^{-1}\text{s}^{-1} \quad (10)$$

These numbers are in good agreement, for example, with apparent association rate constants in the range of 10^5-10^6 M^{-1} s^{-1} for antibodies at a binding capacity of a few thousand RU reported previously (Borrebaeck et al., 1992; Karlsson et al., 1991), or with an apparent association rate

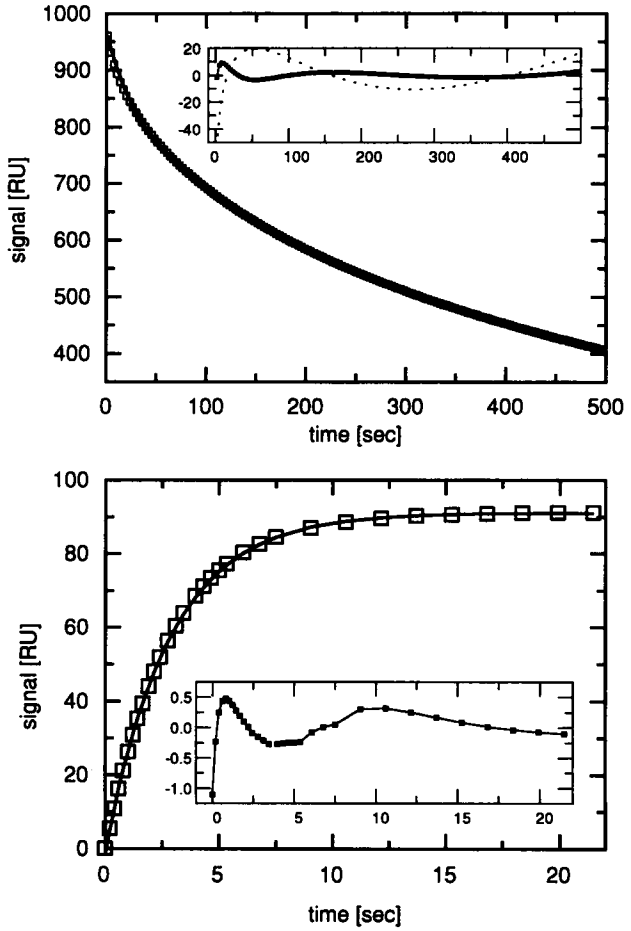

FIGURE 12 (*Upper plot*) Calculated dissociation sensorgram (□) for $k_+ = 500\ (mg/ml)^{-1}{\cdot}s^{-1}$, $k_- = 0.1\ s^{-1}$, $f_0 = 0.01$ mg/ml, $K = 0.3$, $D = 10^{-12}\ m^2/s$, $L = 5 \cdot 10^{-6}$ m/s, $r = 1000$ RU, and double exponential fit to the sensorgram (——) with $k_1 = 0.041\ s^{-1}$ (142 RU), $k_2 = 0.003\ s^{-1}$ (543 RU), and a baseline offset of 285 RU. The inset shows residuals for mono-exponential fit (– – –) and double exponential fit (■). (*Lower plot*) Calculated association sensorgram (□) for $k_+ = 10^4\ (mg/ml)^{-1}{\cdot}s^{-1}$, $k_- = 10^3/s$, $f_0 = 0.01$ mg/ml, $K = 0.3$, $D = 10^{-12}\ m^2/s$, $L = 5 \cdot 10^{-6}$ m/s, $r = 1000$ RU, and mono-exponential fit ($k_{on,\ fit} = 0.351\ s^{-1}$, baseline offset −1.1 RU), assuming apparently ideal binding progress curve (——). The inset shows residuals.

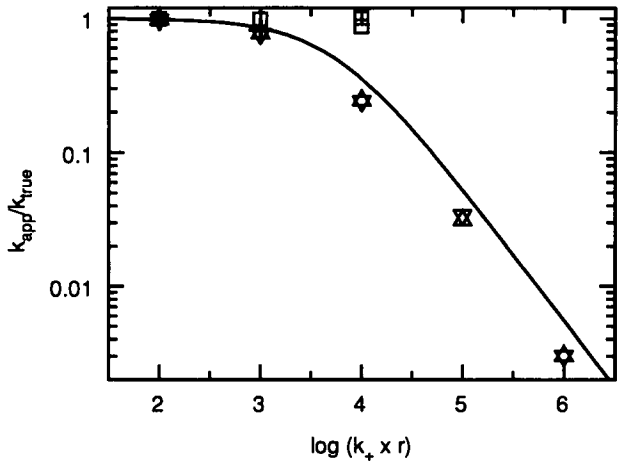

FIGURE 13 Ratio of fitted apparent binding rate k_{app} to ideal binding rate in the absence of transport influence ($k_{true} = k_+ \cdot f_0 + k_-$ for association phase, $k_{true} = k_-$ for dissociation phase) versus log k_+r (in units of $RU \cdot s^{-1} \cdot (mg/ml)^{-1}$). Only sensorgrams that could be fitted by single exponentials (simulated under the conditions of Figs. 6, 7, and 9) were considered. Fits to association sensorgrams with $K_d = 10^{-4}$ mg/ml (+) and $K_d = 0.1$ mg/ml (▽), and to dissociation sensorgrams with $K_d = 10^{-4}$ mg/ml (□) (two values for $k_+ = 10\ (mg/ml)^{-1}{\cdot}s^{-1}$ are with and without baseline offset as a free parameter in the fit) and $K_d = 0.1$ mg/ml (△). Theoretical curve (——) according to Eq. 7.

constant of $4820\ M^{-1}\ s^{-1}$ for a ligand with a molar mass of 45,000 at a binding capacity of >30,000 RU in the study of Ramsdale and co-workers (1993). (Unfortunately, no information about the fraction of receptor incapable of binding is available in this study.) However, it must be emphasized that because of uncertainties in our estimates of the diffusion and the partition coefficients, these estimates in Eq. 10 might be wrong (especially for ligands with very high or low molar mass) by an order of magnitude. Mass transport was found to affect the measured rate constants at reaction rates that are a factor 10–100 lower than those in Eq. 10.

It should be noted that mass transport influences association and dissociation rates by approximately the same factor. Therefore, the quotient k_-/k_+ is more robust. If the influence of mass transport is only moderate, the ratio of k_-^{app}/k_+^{app} can be expected to give approximately correct equilibrium constants K_d, consistent with the value derived from the ligand concentration dependence of the plateau values of the sensorgram. However, for higher transport influence the apparent equilibrium constant will depend considerably on the applied analysis method (cf. Schuck, manuscript submitted for publication).

DISCUSSION

The simulations indicate that diffusion within the gel matrix is at least as important for the measured kinetics as the transport of ligand from the bulk to the gel/bulk interface. In some cases of low diffusion and partition coefficient (high molar mass of ligand and high receptor concentration) it can even be the limiting factor of the binding rate.

Differing estimates of the importance of diffusion within the dextran matrix (cf. Karlsson et al., 1994; Glaser, 1993; Fisher et al., 1994) arise mainly from the fact that the hindrance of diffusion by binding has not been taken into account. In the literature of surface plasmon resonance biosensors, hindered transport was considered only for the interpretation of dissociation data, when rebinding of ligand occurred. Considering the finite volume of the dextran matrix, where the receptor is either homogeneously distributed or occurs in decreasing concentrations toward the gel/bulk interface (Stenberg et al., 1991), it appears that this rebinding should occur mainly within the gel (during the transport toward the gel/bulk interface) rather than during the transport in the bulk phase. But because the retardation of the effective mobility by binding does not depend in principle

on the direction of the transport, diffusion within the matrix also plays an important role in the association phase. Conceptually, the rebinding effect and hindered diffusion in a medium with immobilized receptor are identical.

The mobility of the ligand in the gel matrix is changed because of three different effects that can be described in a mechanical picture. First, large ligand molecules will not be able to enter the gel in the same concentration as in the bulk because of an increased activity coefficient. Because the activity of the ligand is independent of position at equilibrium, this effect does not influence the binding equilibrium, but it influences the material transport inside the gel. Second, in general the presence of polymer chains reduces the diffusion coefficients of tracer particles. Third, and most important, the transport fluxes in the gel are reduced by the amount of binding fluxes to the immobilized receptor, leading to considerably smaller effective diffusion rates. An estimate for the order of magnitude of this effect is the factor $(1 + rk_+/k_-)^{-1}$, because this number is equal to the average time per second in which the ligand is not frozen in its position due to binding to the immobilized receptor (with [bound]/[free] = $t_{trapped}/t_{free}$, and assuming that the binding is rapid compared to the transport). With high receptor concentrations on the order of 10 mg/ml (and more) and dissociation constants in the nanomolar range, effective diffusion can be reduced by more than three orders of magnitude.

Comparison of the simulations with experimental data

Typical effects of mass transport within the matrix can be found in details of the published biosensor data. The most important experimental support for the existence of an inward-traveling front of receptor saturation is an increasing slope in the association phase, because this phenomenon cannot be explained on the basis of transport-influenced binding with homogeneous ligand and receptor distribution inside the gel (except with cooperative binding models; see below). Data with increasing slopes in the association phase under transport influenced conditions are reported, for example, in the studies of Felder et al. (1993), Fisher et al. (1994), Karlsson et al. (1991), van der Merwe et al. (1993), Parsons et al. (1995), Takano et al. (1994, 1995, figure 4), and Yang et al. (1994). In some cases (e.g., Jönsson et al., 1993) it is also visible in the sensorgram of the receptor immobilization step. But although immobilization is an irreversible process, increasing slopes are not found in every case. Possible reasons for the absence could be nonuniform dextran density (de Gennes, 1980) or activation and changes in the structure and optical behavior of the matrix during the immobilization (cf. Stenberg et al., 1991).

That the increasing slopes are associated with very high chemical on rates is supported by the data of Felder et al. (1993). In this study, the addition of a small peptide to the dissociation buffer as competing ligand preventing rebinding made possible an analysis of the chemical off rate. Combined with the equilibrium constant as determined from the plateau values of a set of binding progress curves, chemical on rates of up to $4{\cdot}10^8$ M^{-1} s^{-1} were observed. For on rates in this range (and at the given immobilization level) the appearance of increasing slopes is consistent with the present simulations.

Although the phenomenon of increasing slopes in the association phases remains generally unexplained in the literature, Fisher et al. (1994) have interpreted their observations of this phenomenon as indicative of cooperative binding. In the following these data and the given interpretation will be discussed in some detail.

Fisher and co-workers used a compartment model (distinguishing the location of the ligand inside and outside the gel) to account for material transport from the bulk flow into the gel, which obviously seriously influenced the binding. To be able to fit the increasing slopes of the association phase, they included a positive "steric cooperativity" of neighboring bound ligands in their model. In the attempt to achieve a global fit of the data with different receptor concentrations and inspired by inspection of the data, they took a "surface crowding" effect into account by normalizing the data with respect to the receptor concentration. Additionally, a second binding site was introduced with negative cooperativity, also subject to the surface crowding. Diffusional transport was considered to be fast: in careful observation of the data, initial shoulders on the sensorgram (figure 3 of Fisher et al., 1994) were found and interpreted as signal during the time that is needed for the formation of steady-state conditions with respect to the diffusion above the gel/bulk interface. It was concluded that the signal reaches "apparent equilibrium with respect to diffusion" after 8 ± 1 s, neglecting diffusion inside the gel matrix. In a global fit with an altogether seven unknown rate constants, they found a relatively slow on rate ($\sim$13 $(mg/ml)^{-1}{\cdot}s^{-1}$ for the ligand binding site with positive cooperativity).

The concept of a relatively slow reaction that exhibits cooperativity could in principle qualitatively describe the observed phenomenon. However, the consideration of diffusion within the gel matrix permits a more consistent picture. As shown in the present paper, a traveling saturation boundary (Fig. 3) can produce sensorgrams exhibiting increasing slopes without cooperative binding (Fig. 4). The initial shoulders on the signal can be explained in a more internally consistent way by Eq. A10: after the initial 8 s, the diffusion within the gel becomes significant and decreases the binding rates (Fig. 8) (until it rises again when the saturation front reaches the more sensitive regions). A further congruence of the data with predictions from the moving saturation boundary model is the constancy of the product $T_{plat} * f_0/S_{plat}$ for all data shown that reach the plateau (where T_{plat} denotes the time to reach the plateau signal S_{plat}, and f_0 denotes the bulk ligand concentration). Theoretically, this relation can be found with Eq. A11 at $B = 0$. Furthermore, the dependence of the sensorgram on the flow rate shown in Fig. 2 of Fisher et al. (1994) could fit in

the picture. As in the simulations, the transport from bulk to the gel/bulk interface can change the time scale but not the shape of the sensorgram (Fig. 5).

This shows that the data presented by Fisher et al. (1994) can be explained consistently without the necessity of introducing ad hoc cooperativity and surface crowding effects. In theory, it is possible to resolve ambiguity between a slow cooperative and a fast binding, if a slight ascent of the signal in the dissociation phase after incomplete association phase is observed (Fig. 10), because in the dissociation phase of even a cooperative binding the total number of ligands inside the gel cannot increase. Unfortunately, from figure 1 of Fisher et al. (1994) it is not possible to determine unambiguously whether, for example, the sensorgram for 50-nM ligand on the 274-RU surface shows this slow ascent.

It would be possible in principle to fit the data of Fisher et al. (1994) with numerical solutions of Eqs. 1 and 2, but the results would be meaningless. In the interpretation presented here, these sensorgrams contain essentially no information about the binding kinetics at all, but are determined by other factors, such as details of the receptor distribution in the gel (Fig. 5). However, it should be pointed out that the ability to fit the data without invoking cooperative binding does not disprove the cooperativity suggested by Fisher and co-workers.

Other examples of a slight increase of the signal during the dissociation phase, supporting the existence of the simulated rearrangement of ligand near the sensor surface into more sensitive regions, may possibly be detected in the data of Ramsdale et al. (1993), Corti et al. (1994), and Parsons et al. (1995). Possible baseline drift of about the same magnitude constitutes an intrinsic obstacle to the unambiguous detection of this small effect. Nevertheless, it could be the reason for the reproducible small increase in the signal of unknown cause during the dissociation phase after a binding that did not reach equilibrium, as reported in Gershon and Khilko (1995). It is also difficult to detect the diffusion-induced initial shoulder (Fig. 8), which is in general overlaid upon a refractive index mismatch at the buffer change and possibly partially matched by slower initial binding rates until steady-state conditions of the external transport in the bulk flow are reached. Nevertheless, this shape is visible, for example, in Payne et al. (1993) and Takano et al. (1995).

A different type of deviation from ideal pseudo-first-order kinetics found in the majority of the published data on kinetic experiments is biphasic dissociation. In the absence of other indications of sample heterogeneity, the reason for this behavior remains unclear in most of the experimental studies. However, simulated sensorgrams of the dissociation phase always also followed very closely a sum of one or two exponentials (Fig. 12), where the amplitude of a second component is increasing with increasing transport limitation. At first this is surprising, because it is easy to verify that a sum of two exponentials does not analytically solve Eq. 1 (or a discretized two-compartment version of Eq. 1, respectively). If one thinks about the true solution of Eq. 1 for the dissociation phase in terms of an unknown sum of exponentials, it can be expected that it has components over a broad spectrum of decay times. Although double exponential fits can span an intermediate range, very fast and very slow components are not represented. But these are also not observed because of experimental artifacts caused by the buffer change in the steep part of the decay (O'Shannessy et al., 1993), the limited sample interval of the data, and a possible baseline shift caused by refractive index mismatch of the buffers (O'Shannessy et al., 1993). From the data analysis point of view, the phenomenon of the apparent double exponential dissociation is comparable, for example, to the well-known difficulties in analyzing multimodal size distributions in dynamic light scattering (Provencher, 1979) and unraveling multiple species of unknown molar mass in analytical ultracentrifugation (Haschemeyer and Bowers, 1970). It reflects the general property of exponentials that they are highly correlated and that a few exponentials can fit within a small error to a broad variety of smoothly decaying functions (Phillips, 1962; Varah, 1985).

In many of the published biosensor data, mass transport effects could provide a simple explanation for the biphasic decay. This would be consistent, for example, with the findings of Panayotou et al. (1993), Richalet-Sécordel et al. (1994), and Felder et al. (1993) that the multiphasic dissociation became mono-exponential by adding a peptide that blocks the binding site of the ligand in the dissociation buffer (which prevents "rebinding" and eliminates the dependence of Eq. 1b on free ligand by setting $r - b = 0$).

Although the flow rate in the bulk has in many cases an influence on the measured apparent chemical off rates (e.g., described in detail by Wohlhueter et al., 1994), "rebinding" is not necessarily a process on the gel/bulk surface. This is supported, for example, by the data of Malmborg et al. (1992), who found a flow rate dependence only in the first few seconds (which is consistent with Eq. A10), and by Kelley (1994) and Pack et al. (1995), who found multiphasic dissociation to be entirely independent of the flow rate.

One implication of the dependence of the sensorgram on the diffusion coefficient and partition coefficient is a stronger dependence on the ligand size (in Eqs. 5 and 6) than would be expected from the bulk transport alone (Eq. 4). Experimental support for this is difficult to find in the literature, because 1) many of the established analysis methods are not reliable in analyzing transport-limited data and can have different degrees of sensitivity to the influence of diffusion (cf. Schuck, manuscript in preparation), 2) it requires experiments with immobilized receptor of equal binding capacity, and 3) it requires either pure mass transport limited binding or ligands with equal intrinsic rate constants. The latter requirement can be fulfilled if the roles of ligand and receptor are exchanged. With this type of experiment, Morton and co-workers (1994) found 2.5-fold lower on rates, when the roles of ligand (28,500 Da) and receptor (45,100 Da) were reversed, whereas dR/dt-ver-

sus-R plots showed nonlinearities indicating transport limitation. It is difficult to estimate theoretically the ratio of DK of the reaction partners, which determines their respective diffusion rates within the gel matrix. However, the Stokes-Einstein equation $D_0 = kT/6\pi\eta r$ and Eq. 5 can be used (assuming spherical shapes) to compare the products D_0K. Because this does not take into account the size dependence of the reduction of the diffusion coefficients within the gel matrix D/D_0, the ratio of D_0K can be considered as a lower limit for the ratio of DK. With the given molar masses, on this basis a 1.5-fold decrease in the on rate could be explained. But other factors could be involved, as, for example, form factors in the diffusion coefficients, differences in a possible electrostatic interaction with the dextran matrix (Gorti and Ware, 1985), or possible changes in the intrinsic rate constants due to the immobilization procedure or sterical hindrance. In this study the failure of the technique of adding a competing ligand in the dissociation buffer to prevent rebinding could also be explained by a size effect. The high molar mass leads to a corresponding lower diffusion and partition coefficient of the competing ligand, as compared to the small peptides that were successfully used as competing ligands in other studies.

Size dependence was also suggested by Borrebaeck et al. (1992) as an explanation for the measurement of 10-fold higher on rates for Fab fragments as compared to the native antibody. The high immobilization levels and biphasic dissociation indicate the mass transport-limited conditions, prerequisite for diffusion coefficients to affect the sensorgrams. In this case the calculation of D_0K (assuming spherical shapes for both species) would suggest at least a 3.6-fold increase in the apparent rate constants of Fab relative to antibody. Consideration of differing form factors for hindered diffusion and partition coefficient of a compact globular Fab and a large trilobed antibody would be expected to significantly increase the ratio. A systematic increase of the apparent chemical on rate of antibody fragments with decreasing size was reported by Kelley (1994). The $F(ab)'_2$ fragment showed a 1.5-fold faster on rate than the native antibody, which would be consistent with a theoretical factor of at least 1.8 for total transport-limited rates. However, the off rates showed no consistent trend but varied within a factor 2, probably because of the ambiguity of the analysis of the dissociation phase in the presence of transport limitation (cf. Schuck, manuscript submitted for publication). Additionally, size dependence could be one explanation for lower dissociation rates of a tetrameric miniantibody (tetravalent, molar mass 130,000), as compared to its dimeric form (divalent, molar mass 65,000), in the study of Pack et al. (1995). The observation that the flow rates required for independence of the observed sensorgrams on the buffer flow were higher for the tetrameric form (16 μl/min) than for the dimeric form (8 μl/min) supports the contributing role of differing diffusion coefficients. (Theoretically, with Eq. 4, $D \approx 1/r$ and $r \approx M^{1/3}$, 13 μl/min would lead to the same bulk transport rate for the tetramer as 8 μl/min for the dimer.) The association and dissociation rates were also dependent on the amount of immobilized receptor and significantly lower than measured with NMR on monomeric form, indicating mass transport limitation.

Another consequence of mass transport within the matrix is a buffer and charge dependence, because they possibly alter the interaction of the ligand with the charged dextran chains. This in turn could lead to modification in the diffusion coefficient (Gorti and Ware, 1985). Buffer effects have been frequently observed in experiments (Morton et al., 1994; Poiesi et al., 1993; Tosser et al., 1994; Parsons et al., 1995). But even if transport influence is indicated, for example, by unexplained biphasic dissociation (Morton et al., 1994; Poiesi et al., 1993; Parsons et al., 1995), these buffer and charge effects on the ligand transport could also be caused by a variation in the thickness and density of the dextran matrix, which is pH and ionic strength dependent (Löfås and Johnsson, 1990) due to osmotic effects. They could be combined with and be overlaid on the direct effects of pH and ionic strength on the receptor-ligand interaction. Charge effects on the diffusion coefficient due to electrostatic interaction with the dextran chains could be the reason that a highly charged competing peptide in (Takano et al., 1994) did accelerate but could not completely eliminate the biphasic dissociation.

Limitations of the simulations

Although the simulation model employed considers some major properties of the binding measurement within a gel matrix of immobilized receptor, it is far from being realistic or even complete. One obvious simplification is the reduction to one dimension. In computer simulations, Glaser (1993) has shown that the distribution of ligand in the buffer flow parallel to the sensor surface can seriously influence the binding (treated as pure surface binding) and produce nonlinearities in a dR/dt-versus-R plot. He found deviations from ideal binding and a phase of increasing slope for high on rates and high final receptor saturation. As in the present simulations at low ligand concentrations, even an entirely mass transport-controlled reaction could not be distinguished from exponential binding on the basis of the sensorgrams alone. His calculations are complementary to those presented here, and it can be assumed that the described deviations from ideal binding are superimposed upon those described in the present paper. The much lower ligand mobility in the gel makes it very likely that nonuniformities (with respect to a plane parallel to the sensor) of the initial ligand distributions at the surface of the gel would persist in the form of nonuniform binding profiles in the gel matrix. In general the effects produced by the transport in the flow chamber can be avoided by higher flow rates (Glaser, 1993), whereas the effects of diffusion within the gel matrix cannot.

The assumption that gel and ligand properties are unaffected by receptor and ligand concentrations and indepen-

dent of position within the gel is an oversimplification. First, according to Stenberg et al. (1991), the sensitivity distribution changes with protein inside the gel matrix. The sensitivity decay toward the gel/bulk surface is higher with increasing concentration of bound protein, hence amplifying the observed effects. Second, the diffusion coefficient will be dependent on the local concentration of macromolecules. Third, the gel matrix is not of uniform density (de Gennes, 1980).

Furthermore, it could be speculated that at immobilization levels up to 100 mg/ml and more (based on a 100-nm thickness of the gel) (Calakos et al., 1994; Malmborg et al., 1992; Pack et al., 1995; Natsume et al., 1994; Jönsson et al., 1991; George et al., 1995), binding of large ligands could affect the structure of the dextran chains, e.g., increasing the thickness of the gel matrix to avoid crowding of the interior. The dextran chains are highly flexible and any substantial rearrangement would be visible in the sensorgram. Such effects would become important, especially when the receptor is not directly bound to the dextran, but is captured by a high concentration of immobilized antibodies (e.g., Johne et al., 1993; Mani et al., 1994). Dynamical properties of the dextran chains could be dependent on the receptor distribution. Slow rearrangements would offer one of many possible explanations for the observation of an apparently very slow superimposed binding phase or relaxation process (visible, e.g., in the dR/dt-versus-R plot as an asymptotical rather than a linear approach to a zero slope) (Morton et al., 1994; Horenstein et al., 1993; Natsume et al., 1994).

It should be noted that the size of the gel is not precisely known. Stenberg et al. (1991) calculated its maximum thickness to be 220 nm, assuming that the ends of the dextran chains are grafted on the solid surface. Variation of the thickness within the range 100–200 nm, which is the range given by Johnsson et al. (1995), has a significant influence on the ligand transport even at relatively low reaction rates, as can be seen in Fig. 11. The value of 100 nm used in the simulations therefore is a lower limit and the importance of diffusion within the dextran matrix could be much higher. The pH and ionic strength dependence of its thickness (Löfås and Johnsson, 1990) can represent an additional complication.

GENERAL REMARKS

The major conclusion of the present study is that the diffusion of ligand within the dextran gel is at least equally important for the overall mass transport, as the bulk transport and introduces many generally unknown factors into the binding progress curve. Transport limitation in the gel can even be the limiting factor for the binding kinetics and may be very difficult to detect. Because of the contribution of ligand transport within the gel, the binding progress curve is influenced by mass transport at lower chemical rate constants than previously thought. While with relatively slow reactions the ligand distribution within the gel is almost homogeneous, higher reaction rates can result in high inhomogeneities of the ligand distribution and in a number of deviations from the ideal binding progress curves, some of which are difficult to distinguish from complicated reaction schemes. Although the model used in the simulation is simplified in many respects and cannot explain each type of deviation from an ideal sensorgram, it was shown above that there is much evidence that the types of deviations from the ideal observed in the simulations are significant in real experiments.

It has been stated that in the biosensor literature "deviations from linearity are more a rule than an exception" (Karlsson et al., 1994). The simulated sensorgrams start to deviate from apparently ideal binding progress curves when the rate constants are comparable to the transport rates. We suspect that in most of the cases where unexplained biphasic dissociation is observed highly transport influenced chemical rates, if not pure transport rates, were measured instead of true chemical reaction rates. If this is true, many of the reported rate constants may be wrong, some by as much as several orders of magnitude. Because unknown factors such as details of the sensitivity distribution, receptor distribution, ligand size, ligand-dextran interactions, thickness, and dynamic processes of the dextran gel dominate the sensorgram in the region where deviations from ideal behavior are found, even comparative qualitative analyses could reflect differences in transport properties rather than differences in actual reaction rates.

To reduce mass transport effects it would be advantageous to use a considerably thinner dextran matrix, because the size of the gel is the single most important variable for the mass transport within the gel. A lower binding capacity of a gel with considerable lower dextran concentration and shorter dextran chains would in most cases satisfy the need to have low concentrations of immobilized receptor to ensure reaction-controlled kinetics. Alternatively, the receptor could be incorporated in or bound on a supported lipid bilayer (Plant et al., 1995) or on aminosilanized surfaces (Watts et al., 1994). This should be combined with an efficient flow in the bulk phase.

For qualitative and equilibrium binding studies the high sensitivity that is achieved with the dextran matrix is certainly an advantage, but as shown here even an unambiguous qualitative comparative interpretation of fast kinetics can be difficult. With respect to the kinetic analysis, the attainment of a high binding capacity (Löfås et al., 1991; Liedberg et al., 1993) aims in the wrong direction, where a high signal-to-noise ratio is achieved, but the measurement likely reports something totally different yet indistinguishable from reaction rates. This is even more true for the diagnostics and analysis of heterogeneity, charge effects on the binding, and more complicated reaction schemes. Isomerism of antibodies and equilibria between conformations of different kinetic properties were suggested to be a widespread phenomenon (Foote and Milstein, 1994). However, as detected by evanescent wave biosensors in the presence of a dextran

matrix, they can be indistinguishable from or overlaid by artifacts related to the transport.

APPENDIX

Description of the ideal binding progress curve

Neglecting the mass transport and problems connected with the finite volume in which the reaction takes place, an ideal reversible binding of free ligand f to receptor r with pseudo-first-order can be written as

$$\frac{db}{dt} = k_+ f(r - b) - k_- b, \tag{A1}$$

where k_+ and k_- denote the chemical on rate and off rate, respectively, and b denotes the concentration of bound ligand. Assuming that initially no ligand is bound and that the free ligand concentration is kept constant during the binding process by infinite fast exchange with a bulk phase,

$$b(t) = \frac{r}{1 + \dfrac{k_-}{k_+ f}}(1 - e^{-(k_+ f + k_-)t}) \tag{A2}$$

solves the differential equation Eq. A1 and describes the concentration of bound ligand, depending on time during the association phase. For the dissociation phase the concentration of free ligand is zero and

$$b(t) = b(t_0)e^{-k_-(t - t_0)}. \tag{A3}$$

The signal $R(t)$ is assumed to be proportional to the amount of bound ligand $b(t)$ (Stenberg et al., 1991). The binding progress curves $R(t)$ corresponding to Eqs. A2 and A3 are referred to as the ideal binding progress curves.

Numerical procedure

To get a numerical solution of the partial differential equation Eq. 1, the gel was divided into N layers of equal thickness Δz, and a modified Crank-Nicholson method (Crank and Nicholson, 1947) was used. According to Eq. 1, the change Δf of free ligand in each layer during the time increment Δt can be divided into the change due to the material transport $(\Delta f)_{diff}$ and the decrease due to binding Δb.

$$\Delta f = (\Delta f)_{diff} - \Delta b. \tag{A4}$$

To calculate Δb, the existence of an analytical expression for the time course of binding at constant ligand concentration was exploited:

$$(\Delta b)_f = \left(\frac{k_+ fr}{k_+ f + k_-} - b\right)(1 - e^{-(k_+ f + k_-)\Delta t}). \tag{A5}$$

To take into account that the concentration of free ligand in the layer will change during the timestep, the expression Eq. A5 was centered in the ligand concentration during Δt using the following linearization:

$$\Delta b = (\Delta b)_f + \frac{1}{2}\frac{\partial \Delta b}{\partial f}\Delta f. \tag{A6}$$

The derivative in Eq. A6 is taken analytically. It contains simple expressions and the same exponential as in Eq. A5 and therefore can be computed very efficiently. With Eq. A4 and Eq. A6 follows

$$\Delta f = \frac{1}{1 + \dfrac{1}{2}\dfrac{\partial \Delta b}{\partial f}}\left\{(\Delta f)_{diff} - (\Delta b)_f\right\}. \tag{A7}$$

Details of an efficient numeric solution of Eq. A7 for each layer are given in Press et al. (1992).

The use of Eqs. A5 and A7 instead of a direct discretization of Eq. 1 avoids oscillations of the calculated concentrations of free ligand in the case of transport-limited binding at high reaction rates. This allows reasonably high step sizes in all cases.

The step size t of the time evolution was adapted to keep the maximum relative change of free and bound material of all layers in an interval from 2.5% to 10%. This interval, as well as the number of layers N, was changed in preliminary simulation experiments to verify that it provides convergence of the solutions. The resulting time increments vary from $\sim 10^{-12}$ s for fast reaction rates and high initial concentration gradients to ~ 1 s near the equilibrium.

As a control the calculated distribution $b(z, t)$ was tested to fulfill Eq. 1, and the total mass in the gel at any time was tested for the equality with the net fluxes into the gel, summed over all time steps.

Implemented in C++ and running on a 90 MHz PC, the described procedure completes one simulation in approximately 1–2 min. The program with source code is available on request from the author.

Analytical description for exclusively transport controlled binding

As a model for binding with high reaction rates and high saturation, the limit of infinite fast and irreversible binding (up to the concentration $b_{plat}(z)$) is described. For this reaction, the binding is entirely transport controlled: The ligand flux j into the gel causes a layer of receptor at z_b (the position of the moving boundary), with thickness dz to be saturated to the level $b_{plat}(z)$ in a time $dt = b_{plat}(z)dz/j$. If the equilibrium value $b_{plat}(z)$ is reached, the transport through this layer is not hampered any more, because all binding sites are assumed to be saturated. The ligand flux in the gel is proportional to the gradient, which is linear, hence $j = DKf_G/(G - z_b)$ is valid, where K denotes the partition coefficient and f_G the surface concentration directly above the gel. We can then approximate the effect of retardation by the finite transport coefficient in the bulk, L_{bulk}. Under steady-state conditions at the surface,

$$j = DKf_G/(G - z_b) = L_{bulk}(f_0 - f_G), \tag{A8}$$

it is possible to calculate the surface concentration, f_G, and we finally get

$$j = \frac{1}{\dfrac{G - z_b}{DK} + \dfrac{1}{L_{bulk}}} f_0. \tag{A9}$$

Hence, the time increment dt needed to fill the layer at z_b is

$$dt = \frac{b_{plat}(z_b)}{f_0}\left[\frac{G - z_b}{DK} + \frac{1}{L_{bulk}}\right]dz. \tag{A10}$$

Integration from $z_b = B$ to $z_b = G$ gives the time needed for the inward moving boundary to reach the position B,

$$t(B) = \frac{b_{plat}}{f_0}\left[\frac{(G - B)^2}{2DK} + \frac{(G - B)}{L_{bulk}}\right], \tag{A11}$$

and the position of the boundary at a given time:

$$B(t) = G - KD\left\{\sqrt{\frac{1}{{L_{bulk}}^2} + \frac{2f_0}{KDb_{plat}}t} - \frac{1}{L_{bulk}}\right\}. \tag{A12}$$

The time-dependent distribution $b_{transp}(z, t)$ of the binding is

$$b_{transp}(z, t) = \begin{cases} b_{plat} & \text{for } B(t) \le z \le G \\ 0 & z < B(t) \end{cases}. \quad \text{(A13)}$$

Inserted in Eq. 3, this gives a simple expression for the signal $R(t)$ of the exclusively transport controlled irreversible binding.

Compartment model for the consecutive two-step transport and binding process

If we use a compartment model to distinguish the free ligand in the gel (f_G), in the bulk (f_B), and at the gel/bulk interface (f_{sf}), the transport flux densities in the gel (j_G) and in the bulk (j_B) are given by

$$\begin{aligned} j_B &= L_B(f_B - f_{sf}) \\ j_G &= L_G(Kf_{sf} - f_G), \end{aligned} \quad \text{(A14)}$$

where L_G and L_B denote the transport coefficients and K the partition coefficient. This takes into account that the concentration gradients within the gel are reduced by partition coefficients smaller than unity. Under steady-state conditions at the surface, these fluxes are equal and the surface concentration can be eliminated:

$$j_G = \frac{L_G L_B}{L_G K + L_B}(Kf_B - f_G). \quad \text{(A15)}$$

Approximating the activity of the ligand within the gel by the product of concentration and the inverse of the partition coefficient, the reversible binding reaction can be written as

$$\dot{b} = k_+ \frac{f_G}{K}(r - b) - k_- b. \quad \text{(A16)}$$

Again, under steady-state conditions the reaction flux density $j_{react} = Gb$ is equal to the transport flux, leading to an expression for the steady-state concentration of free ligand in the gel:

$$f_G = \frac{\frac{L_G L_B}{L_G K + L_B} K f_B + k_- G b}{\frac{L_G L_B}{L_G K + L_B} + G\frac{k_+}{K}(r - b)}. \quad \text{(A17)}$$

Inserting Eq. A17 into A16 leads to

$$\dot{b} = \frac{1}{1 + k_+(r - b)G\frac{L_G K + L_B}{L_G K L_B}}[k_+ f_B(r - b) - k_- b]. \quad \text{(A18)}$$

With the assumption that the transport distance within the gel is $G/2$, L_G equals $2D/G$. Therefore, in the steady-state approximation of this model the kinetics follows an equation similar to the ideal rate equation (Eq. A1), with apparent reaction rates k_+^{app} and k_-^{app} related to the true reaction rate and transport parameters by

$$\frac{k_+^{app}}{k_+} = \frac{k_-^{app}}{k_-} = \frac{1}{1 + k_+(r - b)G\frac{2DK + GL_B}{2DKL_B}}. \quad \text{(A19)}$$

This equation is analogous to expressions for effective rate constants in diffusion-limited binding to planar surfaces (Balgi et al., 1995) and to spheres (Goldstein and Dembo, 1995). Because a single transport process generally reduces the apparent rate constants under steady-state conditions by the factor $(1 + k_+(r - b)/k_{tr})^{-1}$, Eq. A19 can be used to calculate an effective combined transport rate constant:

$$k_{tr} = \frac{2DKL_B}{G(2DK + GL_B)}. \quad \text{(A20)}$$

The author acknowledges with pleasure Allen Minton for his continuous support and stimulating discussions. He also wants to thank Irwin Chaiken and Don Bennett for an introduction to the practical aspects of biosensor experiments.

Dedicated to the memory of Dr. Martin Zulauf.

REFERENCES

Balgi, G., D. E. Leckband, and J. M. Nitsche. 1995. Transport effects on the kinetics of protein-surface binding. *Biophys. J.* 68:2251–2260.

Borrebaeck, C. A. K., A.-C. Malmborg, C. Furebring, A. Michaelsson, S. Ward, L. Danielsson, and M. Ohlin. 1992. Kinetic analysis of recombinant antibody-antigen interactions: relation between structural domains and antigen binding. *BioTechnology.* 10:697–698.

Buckle, P. E., R. J. Davies, T. Kinning, D. Yeung, P. R. Edwards, D. Pollard-Knight, and C. R. Lowe. 1993. The resonant mirror: a novel optical sensor for direct sensing of biomolecular interactions. Part II: Applications. *Biosens. Bioelectron.* 8:355–363.

Calakos, N., M. K. Bennett, K. E. Peterson, and R. H. Scheller. 1994. Protein-protein interactions contributing to the specifity of intracellular vesicular trafficking. *Science.* 263:1146–1149.

Chaiken, I., S. Rosé, and R. Karlsson. 1992. Analysis of macromolecular interactions using immobilized ligands. *Anal. Biochem.* 201: 197–210.

Cooper, L. J. N, D. Robertson, R. Granzow, and N. S. Greenspan. 1994. Variable domain-identical antibodies exhibit IgG subclass-related differences in affinity and kinetic constants as determined by surface plasmon resonance. *Mol. Immunol.* 31:577–584.

Corti, A., C. Poiesi, S. Merli, and G. Cassani. 1994. Tumor necrosis factor (TNF)α quantification by ELISA and bioassay: effects of TNFα-soluble TNF receptor (p55) complex dissociation during assay incubations. *J. Immunol. Methods.* 177:191–198.

Crank, J. 1975. The Mathematics of Diffusion, 2nd ed. Clarendon Press, Oxford.

Crank, J., and P. Nicholson. 1947. A practical method for numerical evaluation of solutions of partial differential equations of the heat-conduction type. *Proc. Cambridge Phil. Soc.* 43:50–67.

Cush, R., J. M. Cronin, W. J. Steward, C. H. Maule, J. Molloy, and N. J. Goddard. 1993. The resonant mirror: a novel optical biosensor for direct sensing of biomolecular interactions. Part I: Principle of operation and associated instrumentation. *Biosens. Bioelectron.* 8:347–353.

DeLisi, C. 1980. The biophysics of ligand-receptor interactions. *Q. Rev. Biophys.* 13:201–230.

de Gennes, P. G. 1980. Conformation of polymers attached to an interface. *Macromolecules.* 13:1069–1075.

Fägerstam, L. G., Å. Frostell-Karlsson, R. Karlsson, B. Persson, and I. Rönnberg. 1992. Biospecific interaction analysis using surface plasmon resonance detection applied to kinetic, binding site and concentration analysis. *J. Chromatogr.* 597:397–410.

Felder, S., M. Zhou, P. Hu, J. Ureña, A. Ullrich, M. Chaudhuri, M. White, S. E. Shoelson, and J. Schlesinger. 1993. SH2 domains exhibit high-affinity binding to tyrosine-phosphorylated peptides yet also exhibit rapid dissociation and exchange. *Mol. Cell. Biol.* 13: 1449–1455.

Fisher, R. J., and M. Fivash. 1994. Surface plasmon resonance based methods for measuring the kinetics and binding affinities of biomolecular interactions. *Curr. Opin. Biotechnol.* 5:389–395.

Fisher, R. J., M. Fivash, J. Casas-Finet, S. Bladen, and K. L. McNitt. 1994. Real-time BIAcore measurement of *Escherichia coli* single-stranded DNA binding (SSB) protein to polydeoxythymidylic acid reveals single-state kinetics with steric cooperativity. *Methods: A Companion to Methods Enzymol.* 6:121–133.

Foote, J., and C. Milstein. 1991. Kinetic maturation of an immune response. *Nature.* 352:530–532.

Foote, J., and C. Milstein. 1994. Conformational isomerism and the diversity of antibodies. *Proc. Natl. Acad. Sci. USA.* 91:10370–10374.

George, A. J. T., R. R. French, and M. J. Glennie. 1995. Measurement of kinetic binding constants of a panel of anti-saporin antibodies using a resonant mirror biosensor. *J. Immunol. Methods.* 183:51–63.

Gershon, P. D., and S. Khilko. 1995. Stable chelating linkage for reversible immobilization of oligohistidine tagged proteins in the BIAcore surface plasmon resonance detector. *J. Immunol. Methods.* 183:65–76.

Giddings, J. C., E. Kucera, C. P. Russell, and M. N. Myers. 1968. Statistical theory for the equilibrium distribution of rigid molecules in inert porous networks. Exclusion chromatography. *J. Phys. Chem.* 72: 4397–4408.

Glaser, R. W. 1993. Antigen-antibody binding and mass transport by convection and diffusion to a surface: a two-dimensional computer model of binding and dissociation kinetics. *Anal. Biochem.* 213: 152–161.

Goldstein, B., and M. Dembo. 1995. Approximating the effects of diffusion on reversible reactions at the cell surface: ligand-receptor kinetics. *Biophys. J.* 68:1222–1230.

Gorti, S., and B. R. Ware. 1985. Probe diffusion in an aqueous polyelectrolyte solution. *J. Chem. Phys.* 83:6449–6456.

Guichard, G., N. Benkirane, G. Zeder-Lutz, M. H. V. Van Regenmortel, J.-P. Briand, and S. Muller. 1994. Antigenic mimicry of natural L-peptides with retro-inverso-peptidomimetics. *Proc. Natl. Acad. Sci. USA.* 91:9765–9769.

Haschemeyer, R. H., and W. F. Bowers. 1970. Exponential analysis of concentration or concentration difference data for discrete molecular weight distributions in sedimentation equilibrium. *Biochemistry.* 9:435–445.

Horenstein, A. L., C. Poiesi, L. DeMonte, M. Camagna, M. Mariani, A. Albertini, and F. Malavasi. 1993. Real-time kinetic analysis applied to the production of bispecific monoclonal antibodies for radioimmunodetection of cancer. *Int. J. Clin. Lab. Res.* 23:199–205.

Hsieh, H. V., and N. L. Thompson. 1994. Theory for measuring bivalent surface binding kinetics using total internal reflection with fluorescence photobleaching recovery. *Biophys. J.* 66:898–911.

Ito, W., and Y. Kurosawa. 1993. Development of an artificial antibody system with multiple valency using an Fv fragment fused to a fragment of protein A. *J. Biol. Chem.* 268:20668–20675.

Johne, B., M. Gadnell, and K. Hansen. 1993. Epitope mapping and binding kinetics of monoclonal antibodies studied by real time biospecific interaction analysis using surface plasmon resonance. *J. Immunol. Methods.* 160:191–198.

Johnsson, B., S. Löfås, G. Lindquist, Å. Edström, R.-M. Müller Hillgren, and A. Hansson. 1995. Comparison of methods for immobilization to carboxymethyl dextran sensor surfaces by analysis of the specific activity of monoclonal antibodies. *J. Mol. Recogn.* 8:125–131.

Jönsson, U., L. Fägerstam, B. Ivarsson, B. Johnsson, R. Karlsson, K. Lundh, S. Löfås, B. Persson, H. Roos, I. Rönnberg, S. Sjölander, E. Stenberg, R. Ståhlberg, C. Urbaniczky, H. Östlin, and M. Malmqvist. 1991. Real-time biospecific interaction analysis using surface plasmon resonance and a sensor chip technology. *BioTechniques.* 11: 620–627.

Jönsson, U., L. Fägerstam, S. Löfås, E. Stenberg, R. Karlsson, Ä. Frostell, F. Markey, and F. Schindler. 1993. Introducing a biosensor based technology for real-time biospecific interaction analysis. *Ann. Biol. Clin.* 51:19–26.

Karlsson, R., A. Michaelsson, and L. Mattson. 1991. Kinetic analysis of monoclonal antibody-antigen interactions with a new biosensor based analytical system. *J. Immunol. Methods.* 145:229–240.

Karlsson, R., H. Roos, L. Fägerstam, and B. Persson. 1994. Kinetic and concentration analysis using BIA technology. *Methods: A Companion to Methods Enzymol.* 6:99–110.

Kelley, R. F. 1994. Thermodynamics of protein-protein interaction studied by using BIAcore and single-site mutagenesis. *Methods: A Companion to Methods Enzymol.* 6:111–120.

Kooyman, R. P. H., H. Kolkman, J. Van Gent, and J. Greve. 1988. Surface plasmon resonance immunosensors: sensitivity considerations. *Anal. Chim. Acta.* 213:35–45.

Langevin, D., and F. Rondelez. 1978. Sedimentation of large colloidal particles through semidilute polymer solutions. *Polymer.* 19:875–882.

Liedberg, B., I. Lundström, and E. Stenberg. 1993. Principles of biosensing with an extended coupling matrix and surface plasmon resonance. *Sensors Actuators B.* 11:63–72.

Löfås, S., and B. Johnsson. 1990. A novel hydrogel matrix on gold surfaces in surface plasmon resonance sensors for fast and efficient covalent immobilization of ligands. *J. Chem. Soc. Chem. Commun.* 21: 1526–1528.

Löfås, S., M. Malmqvist, I. Rönnberg, E. Stenberg, B. Liedberg, and I. Lundström. 1991. Bioanalysis with surface plasmon resonance. *Sensors Actuators B.* 5:79–84.

Malmborg, A.-C., and C. A. K. Borrebaeck. 1995. BIAcore as a tool in antibody engineering. *J. Immunol. Methods.* 183:7–13.

Malmborg, A.-C., A. Michaëlsson, M. Ohlin, B. Jansson, and C. A. K. Borrebaeck. 1992. Real time analysis of antibody-antigen reaction kinetics. *Scand. J. Immunol.* 35:643–650.

Mani, J.-C., V. Marchi, and C. Cucurou. 1994. Effect of HIV-1 peptide presentation on the affinity constants of two monoclonal antibodies determined by BIAcore technology. *Mol. Immunol.* 31:439–444.

Morton, T. A., D. B. Bennett, E. R. Appelbaum, D. M. Cusimano, K. O. Johanson, R. E. Matico, P. R. Young, M. Doyle, and I. M. Chaiken. 1994. Analysis of the interaction between human interleukin-5 and the soluble domain of its receptor using a surface plasmon resonance biosensor. *J. Mol. Recogn.* 7:47–55.

Natsume, T., T. Koide, S.-i. Yokota, K. Hirayoshi, and K. Nagata. 1994. Interactions between collagen-binding stress protein HSP47 and collagen. *J. Biol. Chem.* 269:31224–31228.

O'Shannessy, D. J. 1994. Determination of kinetic rate and equilibrium binding constants for macromolecular interactions: a critique of the surface plasmon resonance literature. *Curr. Opin. Biotechnol.* 5:65–71.

O'Shannessy, D. J., M. Brigham-Burke, K. K. Soneson, P. Hensley, and I. Brooks. 1993. Determination of rate and equilibrium binding constants for macromolecular interactions using surface plasmon resonance: use of nonlinear least squares analysis methods. *Anal. Biochem.* 212:457–468.

Pack, P., K. Müller, R. Zahn, and A. Plückthun. 1995. Tetravalent miniantibodies with high avidity assembling in *Escherichia coli. J. Mol. Biol.* 246:28–34.

Panayotou, G., G. Gish, P. End, O. Truong, I. Gout, R. Dhand, M. J. Fry, I. Hiles, T. Pawson, and M. D. Waterfield. 1993. Interactions between SH2 domains and tyrosine-phosphorylated platelet-derived growth factor β-receptor sequences: analysis of kinetic parameters by a novel biosensor-based approach. *Mol. Cell. Biol.* 13:3567–3576.

Parsons, I. D., B. Persson, A. Mekhalfia, G. M. Blackburn, and P. G. Stockley. 1995. Probing the molecular mechanism of action of co-repressor in the *E. coli* methionine repressor-operator complex using surface plasmon resonance (SPR). *Nucleic Acids Res.* 23:211–216.

Payne, G., S. E. Shoelson, G. D. Gish, T. Pawson, and C. T. Walsh. 1993. Kinetics of $p56^{lck}$ and $p60^{src}$ Src homology 2 domain binding to tyrosine-phosphorylated peptides determined by a competition assay or surface plasmon resonance. *Proc. Natl. Acad. Sci. USA.* 90:4902–4906.

Phillies, G. D. J. 1985. Diffusion of bovine serum albumin in a neutral polymer solution. *Biopolymers.* 24:379–386.

Phillips, D. L. 1962. A technique for the numerical solution of certain integral equations of the first kind. *J. Assist. Comput. Mach.* 9:84–97.

Plant, A. L., M. Brigham-Burke, E. C. Petrella, and D. J. O'Shannesy. 1995. Phospholipid/alkanethiol bilayers for cell-surface receptor studies by surface plasmon resonance. *Anal. Biochem.* 226:342–348.

Poiesi, C., A. Albertini, S. Ghielmi, G. Cassani, and A. Corti. 1993. Kinetic analysis of the TNF-α oligomer-monomer transition by surface plasmon resonance and immunochemical methods. *Cytokine.* 5:539–545.

Press, W. H., S. A. Teukolsky, W. T. Vetterling, and B. P. Flannery. 1992. Numerical Recipes in C, 2nd ed (corrected 1994). Cambridge University Press, Cambridge.

Provencher, S. W. 1979. Inverse problems in polymer characterization: direct analysis of polydispersity with photon correlation spectroscopy. *Makromol. Chem.* 180:201–209.

Raether, H. 1977. Surface plasma oscillations and their applications. *In* Physics of Thin Films. G. Hass, M. H. Francombe, and R. W. Hoffman, editors. Academic Press, New York. 9:145–261.

Ramsdale, T. E., P. R. Andrews, and E. C. Nice. 1993. Verification of the interaction between peptide T and CD4 using surface plasmon resonance. *FEBS Lett.* 333:217–222.

Richalet-Sécordel, P. M., G. Zeder-Lutz, S. Plaue, G. Sommermeyer-Leroux, and M. H. V. Van Regenmortel. 1994. Cross-reactivity of monoclonal antibodies to a chimeric V3 peptide of HIV-1 with peptide analogues studied by biosensor technology and ELISA. *J. Immunol. Methods.* 176:221–234.

Silhavy, T. J., S. Szmelcman, W. Boos, and M. Schwartz. 1975. On the significance of the retention of ligand by protein. *Proc. Natl. Acad. Sci. USA.* 72:2120–2124.

Sjölander, S., and C. Urbaniczky. 1991. Integrated fluid handling system for biomolecular interaction analysis. *Anal. Chem.* 63:2338–2345.

Stenberg, E., B. Persson, H. Roos, C. Urbaniczky. 1991. Quantitative determination of surface concentration of protein with surface plasmon resonance using radiolabeled proteins. *J. Colloid Interface Sci.* 143: 513–526.

Takano, E., M. Hatanaka, and M. Maki. 1994. Real-time analysis of the calcium-dependent interaction between calmodulin and a synthetic oligopeptide of calcineurin by a surface plasmon resonance biosensor. *FEBS Lett.* 352:247–250.

Takano, E., H. Ma, H. Q. Yang, M. Maki, and M. Hatanaka. 1995. Preference of calcium-dependent interactions between calmodulin-like domains of calpain and calpastatin subdomains. *FEBS Lett.* 362:93–97.

Tosser, G., T. Delaunay, E. Kohli, J. Grosclaude, P. Pothier, and J. Cohen. 1994. Topology of bovine rotavirus (RF strain) VP6 epitopes by real-time biospecific interaction analysis. *Virology.* 204:8–16.

van der Merwe, P. A., M. H. Brown, S. J. Davis, and A. N. Barclay. 1993. Affinity and kinetic analysis of the interaction of the cell adhesion molecules rat CD2 and CD48. *EMBO J.* 12:4945–4954.

Varah, J. M. 1985. On fitting exponentials by nonlinear least squares. *Siam J. Sci. Stat. Comput.* 6:30–44.

Watts, H. J., C. R. Lowe, and D. V. Pollard-Knight. 1994. Optical biosensor for monitoring microbial cells. *Anal. Chem.* 66:2465–2470.

Wohlhueter, R. M., K. Parekh, V. Udhayakumar, S. Fang, and A. A. Lal. 1994. Analysis of binding of monoclonal antibody to a malarial peptide by surface plasmon resonance biosensor and integrated rate equations. *J. Immunol.* 153:181–189.

Yang, H. Q., H. Ma, E. Takano, M. Hatanaka, and M. Maki. 1994. Analysis of calcium-dependent interaction between amino-terminal conserved region of calpastatin functional domain and calmodulin-like domain of μ-calpain large subunit. *J. Biol. Chem.* 269:18977–18984.

Zahn, R., S. E. Axmann, K.-P. Rücknagel, E. Jaeger, A. A. Laminet, and A. Plückthun. 1994. Thermodynamic partitioning model for hydrophobic binding of polypeptides by GroEL. *J. Mol. Biol.* 242:150–164.

Zwanzig, R., and A. Szabo. 1991. Time dependent rate of diffusion-influenced ligand binding to receptors on cell surfaces. *Biophys. J.* 60:671–678.